Latitudinal scaling of aggregation with abundance and its consequences for coexistence in species rich forests

Thorsten Wiegand*, Xugao Wang*, Samuel Fischer, Nathan J. B. Kraft, Norman A. Bourg, Warren Y. Brockelman, Min Cao, Wirong Chanthorn, Chengjin Chu, Stuart Davies, Sisira Ediriweera, C. V. S. Gunatilleke, I. A. U. N. Gunatilleke, Zhanqing Hao, Robert Howe, Mingxi Jiang, Guangze Jin, W. John Kress, Buhang Li, Juyu Lian, Luxiang Lin, Feng Liu, Keping Ma, William McShea, Xiangcheng Mi, Jonathan A. Myers, Anuttara Nathalang, David A. Orwig, Guochun Shen, Sheng-Hsin Su, I-Fang Sun, Xihua Wang, Amy Wolf, Enrong Yan, Wanhui Ye, Yan Zhu, Andreas Huth

1. Thorsten Wiegand: Helmholtz Centre for Environmental Research GmbH – UFZ, Department of Ecological Modelling, Permoserstrasse 15, 04318 Leipzig; German Centre for Integrative Biodiversity Research (iDiv) Halle-Jena-Leipzig, Deutscher Platz 5e, 04103 Leipzig;
2. Xugao Wang: CAS Key Laboratory of Forest Ecology and Management, Institute of Applied Ecology Chinese Academy of Sciences, Shenyang, Liaoning;
3. Samuel Fischer: Helmholtz Centre for Environmental Research GmbH – UFZ, Department of Ecological Modelling, Permoserstrasse 15, 04318 Leipzig;
4. Nathan J. B. Kraft: Department of Ecology and Evolutionary Biology, University of California, Los Angeles, 621 Charles E. Young Drive South, Los Angeles;
5. Norman A. Bourg: U.S. Geological Survey, National Research Program – Eastern Branch, Reston, Virginia
6. Warren Y. Brockelman: National Biobank of Thailand (NBT), National Science and Technology Development Agency, Klong Luang, Pathum Thani
7. Min Cao: CAS Key Laboratory of Tropical Forest Ecology, Xishuangbanna Tropical Botanical Garden, Chinese Academy of Sciences, Kunming
8. Wirong Chanthorn: Department of Environmental Technology and Management, Faculty of Environment
9. Chengjin Chu: State Key Laboratory of Biocontrol, School of Ecology, Sun Yat-sen University, Guangzhou
10. Stuart Davies: Forest Global Earth Observatory (ForestGEO), Smithsonian Tropical Research Institute, P.O. Box 37012, Washington DC
11. Sisira Ediriweera: Department of Science and Technology, Uva Wellassa University, Badulla
12. C. V. S. Gunatilleke: Department of Botany, University of Peradeniya, Kandy
13. I. A. U. N. Gunatilleke: Department of Botany, University of Peradeniya, Kandy
14. Zhanqing Hao: School of Ecology and Environment, Northwestern Polytechnical University, Xi'an
15. Robert Howe: Department of Natural and Applied Sciences, University of Wisconsin–Green Bay, 2420 Nicolet Drive, Green Bay, Wisconsin
16. Mingxi Jiang: Key Laboratory of Aquatic Botany and Watershed Ecology, Wuhan Botanical Garden, Chinese Academy of Sciences, Wuhan
17. Guangze Jin: Center for Ecological Research, Northeast Forestry University, Harbin
18. W. John Kress: Department of Botany, National Museum of Natural History, Smithsonian Institution, Washington, DC
19. Buhang Li: State Key Laboratory of Biocontrol, School of Ecology, Sun Yat-sen University, Guangzhou

20. Juyu Lian: Key Laboratory of Vegetation Restoration and Management of Degraded Ecosystems, South China Botanical Garden, Chinese Academy of Sciences, 510650, Guangzhou
21. Luxiang Lin: CAS Key Laboratory of Tropical Forest Ecology, Xishuangbanna Tropical Botanical Garden, Chinese Academy of Sciences, Kunming
22. Feng Liu: Administration Bureau of Naban River Watershed National Nature Reserve, Jinghong, Yunnan 666100, Kunming
23. Keping Ma: State Key Laboratory of Vegetation and Environmental Change, Institute of Botany, Chinese Academy of Sciences, 20 Nanxincun, Xiangshan, Beijing
24. William McShea: Conservation Ecology Center, Smithsonian Conservation Biology Institute, Front Royal, Virginia
25. Xiangcheng Mi: State Key Laboratory of Vegetation and Environmental Change, Institute of Botany, Chinese Academy of Sciences, 20 Nanxincun, Xiangshan, Beijing
26. Jonathan A. Myers: Department of Biology & Tyson Research Center, Washington University in St. Louis, St. Louis, Missouri
27. Anuttara Nathalang, National Biobank of Thailand (NBT), National Science and Technology Development Agency, Klong Luang, Pathum Thani.
28. David A. Orwig: Harvard Forest, Harvard University, Petersham, Massachusetts
29. Guochun Shen: Zhejiang Tiantong Forest Ecosystem National Observation and Research Station, School of Ecological and Environmental Sciences, East China Normal University, Shanghai
30. Sheng-Hsin Su: Taiwan Forestry Research Institute, Taipei
31. I-Fang Sun: Center for Interdisciplinary Research on Ecology and Sustainability, National Dong Hwa University, Hualien
32. Xihua Wang: Zhejiang Tiantong Forest Ecosystem National Observation and Research Station, School of Ecological and Environmental Sciences, East China Normal University, Shanghai
33. Amy Wolf: Department of Natural and Applied Sciences, University of Wisconsin–Green Bay, 2420 Nicolet Drive, Green Bay, Wisconsin
34. Enrong Yan: Zhejiang Tiantong Forest Ecosystem National Observation and Research Station, School of Ecological and Environmental Sciences, East China Normal University, Shanghai
35. Wanhui Ye: Key Laboratory of Vegetation Restoration and Management of Degraded Ecosystems, South China Botanical Garden, Chinese Academy of Sciences, 510650, Guangzhou
36. Yan Zhu: State Key Laboratory of Vegetation and Environmental Change, Institute of Botany, Chinese Academy of Sciences, 20 Nanxincun, Xiangshan, Beijing
37. Andreas Huth: Helmholtz Centre for Environmental Research GmbH – UFZ, Department of Ecological Modelling, Permoserstrasse 15, 04318 Leipzig; German Centre for Integrative Biodiversity Research (iDiv) Halle-Jena-Leipzig, Deutscher Platz 5e, 04103 Leipzig; University Osnabrueck, Institute of Environmental Systems Research, Barbarastrasse 12, 49076 Osnabrueck.

*Correspondence should be addressed to: thorsten.wiegand@ufz.de and wangxg@iae.ac.cn

Abstract

The complex spatial structure and dynamics of ecological communities continue to defy explanation by simple principles despite decades of attention from ecologists and theoreticians. For example, the relationship between plant spatial distributions and species coexistence is often challenging to resolve in empirical settings. By analysing the spatial patterns of trees in 21 large forest plots we find a general and strong latitudinal gradient in the relationship between conspecific aggregation and abundance of tree species, with stronger negative abundance-dependency as latitude increases. To derive theoretical expectations for how interactions between multiple spatial pattern and processes can impact species coexistence, we incorporate the observed spatial patterns together with neighbourhood crowding competition into a mathematical model to estimate the local extinction risk of species. Strikingly, we find simple relationships that predict species local extinction risk from their demography and spatial distribution. Compared to a corresponding non-spatial analysis, accounting for spatial patterns reduces the 1000-year extinction risk on average by 52% when species invade from low abundances of 50 individuals. Additionally, based on their current abundances, only 8% of the species had an extinction risk greater than 5%. Our approach opens up new avenues for integrating observed spatial patterns with multiple ecological processes into mathematical theory. Our results demonstrate that emerging spatial patterns can contribute substantially to coexistence in species-rich forests, emphasizing the need to understand the interacting multiple processes underpinning spatial patterns in greater detail than has previously been appreciated.

Main Text

The maintenance of high species diversity in species-rich communities like tropical forests has fascinated ecologists for decades, but still remains a key challenge for ecological theory (Barabás et al. 2018; Wiegand et al. 2021; Gibbs et al. 2022). Despite of a large number of studies devoted to forests, mechanistic connections among important features of forests and species coexistence are not fully understood. Of crucial importance are the spatial patterns of conspecific aggregation, which have been used for decades to infer mechanisms contributing to the coexistence of tree species in tropical forests (e.g., Janzen 1970; Connell 1971; Hubbell 1979; Sterner et al. 1986; Condit et al. 2000; Comita et al. 2010; Uriarte et al. 2010; Fortunel et al. 2018) because they are related to ecological processes such as negative conspecific density dependence (Janzen 1970; Connell 1971; Sterner et al. 1986; He and Duncan 2000), dispersal limitation (Bleher et al. 2002; Seidler and Plotkin 2006), and habitat filtering (Getzin et al. 2008; McFadden et al. 2019).

Conspecific spatial aggregation describes the increase in the number of conspecific neighbours within a given neighbourhood, compared to the expectation of a random distribution of the species (Wiegand and Moloney 2014). Theoretical and observational studies suggest that conspecific aggregation should relate to abundance, with rarer species showing higher levels of aggregation (e.g., Hubbell 1979; Condit et al. 2000; Bleher et al. 2002; Réjou-Méchain et al. 2011; Flügge et al. 2012; May et al. 2016; Wiegand et al. 2021), whereas others find no significant or only weak relationship between aggregation and species abundance (e.g., He et al. 1997; Plotkin et al. 2000). However, while stronger conspecific aggregation increases the strength of conspecific competition relative to heterospecific competition and may therefore promote coexistence (Chesson 2000), it is less recognized that a negative relationship between aggregation and abundance can also destabilize coexistence (Wiegand et al. 2021; Ellner et al. 2022). In this case the rare species advantage required for coexistence does not emerge because rarer species do not escape intense conspecific competition since their local densities do not decline sufficiently with decreasing abundance (Klausmeier and Tillman 2002; Wiegand et al. 2021; Ellner et al. 2022). Thus, conspecific spatial aggregation is related in non-trivial ways with species coexistence, but the role of spatial patterns play in shaping coexistence is still poorly explored (Detto and Muller-Landau 2016; Wiegand et al. 2021).

Here, we conduct a comprehensive analysis of spatial neighbourhood patterns of trees in forests along latitude and integrate this information into mathematical theory to investigate geographic variation in species coexistence, resulting from reduced tree survival in areas of high local density of neighbours (i.e., neighbourhood crowding; Box 1), e.g., through competition for space, light or nutrients (Lewis et al. 2000), or natural enemies (Janzen 1970; Connell 1971; Mangan et al. 2010). To this end, we derive theoretical expectations for how multiple spatial neighbourhood patterns (such as aggregation-abundance relationships and heterospecific neighbourhood crowding), derived from large step-mapped forest inventories (Davies et al. 2021), interact with multiple ecological processes (such as negative density dependence, demographic stochasticity, and differences in niche overlap among species) in determining the local extinction risk of species in empirical settings.

Box 1. Crowding indices, aggregation, segregation, and link with macroscale dynamics

conspecifics:	$C_{kf} = \sum_{j=1}^{n_f} \frac{1}{d_{kj}}$	$k_{ff} = \overline{C_{kf}}/(c\, N_f)$	(a)
heterospecifics:	$H_{kf} = \sum_{i \neq f} \sum_{j=1}^{n_i} \frac{1}{d_{kj}}$	$k_{fh} = \overline{H_{kf}}/(c \sum_{i \neq f} N_i)$	(b)
niche differences:	$I_{kf} = \sum_{i \neq f} \sum_{j=1}^{n_i} \frac{\beta_{fi}}{\beta_{ff}} \frac{1}{d_{kj}}$	$\overline{I_{kf}} = k_{fh} B_f (c \sum_{s \neq f} N_s)$, $B_f = \frac{\overline{I_{kf}}}{\overline{H_{kf}}}$	(c)
survival:	$s_{kf} = s_f e^{-\beta_{ff}(C_{kf} + I_{kf})}$	$\bar{s}_f = s_f e^{-\beta_{ff}(\gamma_{ff}\overline{C_{kf}} + \gamma_{f\beta}\overline{I_{kf}})}$	(d)

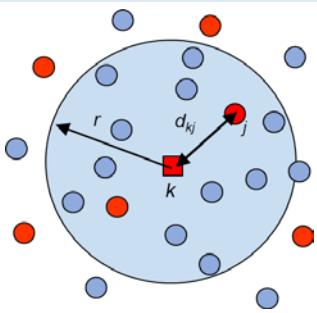

We assume that the survival of an individual k (red square) depends on the proximity of con- and heterospecific neighbours j within its neighbourhood with radius r (blue shaded area), as described by "neighbourhood crowding indices" (*NCI*'s; Canham et al. 2004; Uriarte et al. 2004, 2010).

The crowding index C_{kf} counts all conspecifics j of species f (red circles) with distances $d_{kj} < r$ within the neighbourhood of the focal individual k, but weights them by $1/d_{kj}$ (eq. a), assuming that distant neighbours compete less. The crowding index H_{kf} does the same with all heterospecifics (blue disks) (eq. b), and the crowding index I_{kf} weights heterospecifics of species i additionally by their relative competition strength β_{fi}/β_{ff} (eq. c).

The **population averages** $\overline{C_{kf}}$ (abbreviated $\boldsymbol{C_{ff}}$) **and** $\overline{I_{kf}}$ (abbreviated $\boldsymbol{I_{fh}}$) of the crowding indices determine the **average survival rate** $\bar{s}_f$ that drives dynamics at the community scale (eq. d; eq. 8 in methods). In addition, we quantify patterns in the placement of conspecifics (k_{ff}) and heterospecifics (k_{fh}) in the neighbourhood of the focal species f by dividing the average crowding indices C_{ff} and H_{fh} by their expectation without spatial patterns (eqs. a, b). Thus, **aggregation** describes an increase in conspecific neighbours compared to that of random reference patterns (i.e., $k_{ff} > 1$), and **segregation** ($k_{fh} < 1$) describes an decrease in heterospecific neighbours compared to independently placed heterospecifics.

The quantity B_f (eq. c) is the **average competition strength of one heterospecific neighbour** relative to that of one conspecific and quantifies the average niche differences of the focal species f to heterospecifics. B_f is highly correlated to the mean of β_{fi}/β_{ff} taken over all heterospecific individuals, where $\boldsymbol{\beta_{fi}}$ **is the individual-level interaction coefficient** that measures the negative impact of one neighbour of species i on survival of individuals of the focal species f. We compare two scenarios for β_{fi}, one where con- and heterospecifics compete equally ($\beta_{fi}/\beta_{ff} = 1$), and one with phylogenetic similarity as proxy for β_{fi}/β_{ff}, given that is unfeasible in practise to estimate the β_{fi}/β_{ff} 's for species rich forests (e.g., Canham et al. 2006). N_f is the abundance of species f in a plot of area A, c is a scaling factor ($c = 2\,\pi\, r/A$).

Using data of 720 tree species in 21 large temperate, subtropical and tropical forest plots from a global network of forest research plots (CTFS-ForestGEO; Davies et al. 2021) (Supplementary Table 1) we find that conspecific aggregation k_{ff} of a species f generally depends negatively on its abundance N_f with power law $k_{ff} = a_f\, N_f^{b_f}$ where the exponent b_f is always negative (Figure 1, Extended Data Fig. 1). Strikingly, the exponents b_f follow a strong latitudinal gradient (Figure 1C, Extended Data Fig. 2). This means that for tropical forests aggregation shows only a weak negative dependency on abundance (Figure 1a), whereas temperate forest tends to show strong negative aggregation-abundance relationships (Figure 1b). As expected by the distance-weighting of the NCI's (Box 1), the strength of the latitudinal gradient was (for neighbourhood radii > 10m) basically independent on the neighbourhood area over which conspecific aggregation is measured (Extended Data Fig. 2).

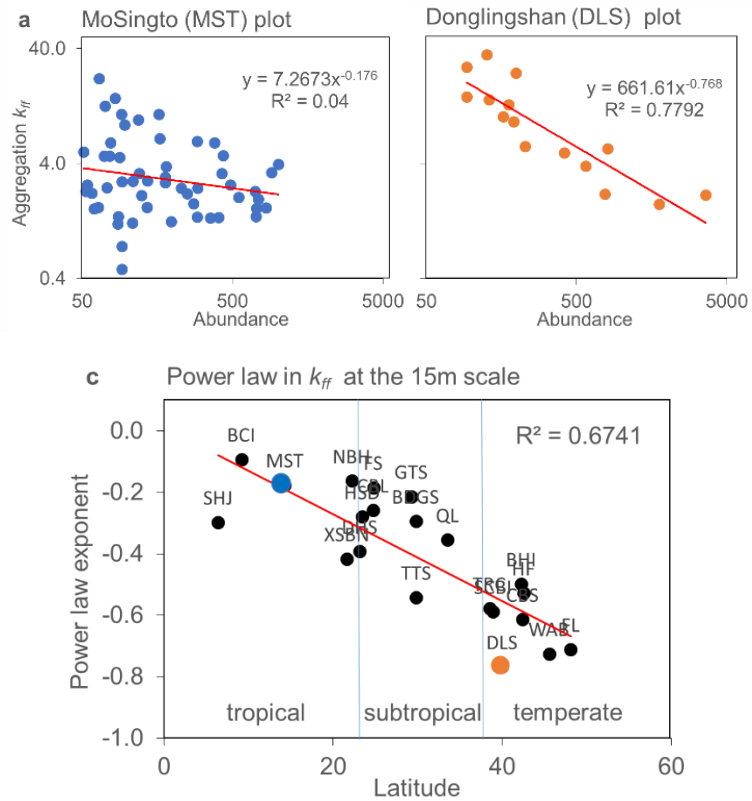

Figure 1. **Geographic variation in the scaling of conspecific aggregation with abundance**. **a,** example of the tropical MoSingto plot, **b**, example of the temperate Donglingshan forest, **c**, latitudinal gradient in the exponent b_f of the relationship between aggregation and abundance for the 21 forest plots. Aggregation is defined in Box 1 (eq. a) and is estimated for neighbourhoods of 15m. We use in our analyses 720 species with at least 50 large trees (diameter at breast height (dbh) ≥ 10cm; Condit et al. 2000). For plot characteristics and acronyms see Supplementary Table 1.

Our results therefore indicate that conspecific neighbourhood densities, which drive crowding competition and are proportionally to aggregation times abundance (eq. a in Box 1), tend to increase in forests at low latitudes linearly with abundance, a pattern which results in negative-frequency dependence which results in negative-frequency dependence if one conspecific neighbour competes on average stronger than one heterospecific neighbour (this was the case for our 720 selected species; Extended Data Fig. 3). However, this frequency dependence becomes weaker in forests at higher latitudes as the exponent approaches values of −1 (Fig. 1B), and it disappears if the exponent reaches values of −1, when local conspecific crowding is independent on abundance. In contrast, we did not find such abundance dependency in the placement of heterospecifics (k_{fh}) in the neighbourhood of focal species f (except for some weaker correlations at temperate forests; Extended Data Fig. 2C). This means that the tendency of focal species to segregate or

be independently placed with respect to individuals of other species was not related to its abundance.

The latitudinal gradient in the relationship between aggregation and abundance we report here (Figure 1c) and absence of such a relationship for heterospecifics are intriguing patterns that suggests that simple principles may underlie the complex spatial structure and dynamics of ecological communities across latitudinal gradients. However, understanding the role of the observed variation in aggregation for species coexistence requires a dynamic model that derives crowding competition mechanistically from the spatial patterns at the scale of individual trees. Upscaling of the critical information on (observed) spatial patterns at the individual level (i.e., the microscale) into phenomenological models that use species abundances as state variables (i.e., macroscale models) is a major challenge (Wiegand et al. 2021).

To evaluate geographic variation in potential coexistence driven by spatial patterns, we use a "spatially-enriched" macroscale model (Wiegand et al. 2021) that incorporates the critical information on spatial pattern at the microscale of individual trees provided by the ForestGEO data sets. Our model assumes that survival of individual trees of a focal species f is reduced in areas of high local density of con- and heterospecifics (i.e., neighbourhood crowding), as described by "neighbourhood crowding indices" (*NCI*'s; Canham et al. 2004; Uriarte et al. 2004, 2010), while reproduction is density-independent with per capita rate r_f (e.g., Detto and Muller-Landau 2016):

$$\frac{N_{f,t+\Delta t}-N_{f,t}}{\Delta t}\frac{1}{N_{f,t}} = \tilde{\lambda}_f\left(N_{f,t}\right) = r_f - (1 - s_f exp(- \beta_{ff} W_f)), \qquad (1)$$

where $N_{f,t}$ is the abundance of species f at time t, Δt the time interval of 5 years between censuses of the ForestGEO plots, the function $\tilde{\lambda}_f\left(N_f\right)$ is the average individual fitness (Chesson 2012), s_f a density-independent per capita background survival rate, and β_{ff} the conspecific individual-level interaction coefficient. The "fitness factor" W_f (Chesson 2012) is in our case the average of the sum of con- and heterospecific neighbourhood crowding $C_{kf} + I_{kf}$ taken over all individuals k of species f (Box 1, eq. d), and it is a function of the species abundance N_i of all species i in the community, spatial patterns, and the aggregation-abundance relationship (equation 6). Separating con- and heterospecific crowing allows us to quantify the relative strength of con- to heterospecific competition. Note that the special case where survival is independent on neighbourhood crowding (i.e., $\beta_{ff} = 0$ or $W_f = 0$; $s_f = 1 - r_f$ in equation 1) results in a neutral model (Hubbell 2001) without immigration, emigration and speciation that shows for all abundances an average individual fitness of zero.

Our spatially-enriched model can be parameterized by the detailed information on spatial patterns of our 21 forest plots from the ForestGEO network (see methods). A crucial insight used in our approach is that crowding competition at the individual scale (equation 4) leads in species rich communities (close to a quasi-stationary state) at the population scale in good approximation to diffuse competition, represented by the quantity B_f, which is the average competition strength of one heterospecific neighbour of species *f*, relative to that of one conspecific neighbour (Wiegand et al. 2021). This allows us to decouple the dynamics of individual species (equation 6c), given that strong local negative density dependence leads in good approximation to zero-sum dynamics (Hubbell 2001), and to replace the multispecies fitness factor W_f of equation 1 by the single-species fitness factor of equation 7b.

To derive a suitable measure of the potential for coexistence of individual species, we used the local risk of extinction of a species within the isolated local community defined by the ForestGEO plot (i.e., no immigration or emigration), relative to the expectation of the corresponding neutral model with average individual fitness $\tilde{\lambda}_f(N_{f,t}) = 0$. More technically, we achieved this by translating our spatially-enriched macroscale model (equation 9) into the stochastic framework of Markov processes of the birth-death type (Azaele et al. 2006). The birth-death model is based on the probabilities that one birth or one death event happens within a small timestep. The corresponding birth and death rates (equation 12) are derived from the average individual fitness, and the birth-death model uses deterministic equations (equation 13) to describe the dynamics of the probability $P_n(t, N_0)$ that a species with initially N_0 individuals has at timestep *t* abundance *n*. Especially, $P_0(t, N_0)$ is the probability that the species is extinct at timestep *t* (Grimm and Wissel 2004). The extinction probability $P_0^n(t, N_0)$ of the corresponding neutral model with per capita reproduction rate r_f and absence of immigration or speciation (equations 12a, c) is well known (e.g., Bailey 1964; Fig. 2A) and serves here as point of reference

$$P_0^n(t, N_0) = \left(\frac{t\ r_f}{1+t\ r_f}\right)^{N_0} \tag{2a}$$

that allows us to directly assess the potential effects of neighbourhood crowding on the ability of species to persist by estimating the relative extinction probability $P_0(t, N_0)/P_0^n(t, N_0)$. If the extinction risk of species is similar to that of the neutral model, we call this species "near neutral". As a rough "over the thumb" indicator we use a 50 % reduction in the extinction risk as threshold, thus a species behaves near-neutral if $P_0(t, N_0) > 0.5\ P_0^n(t, N_0)$.

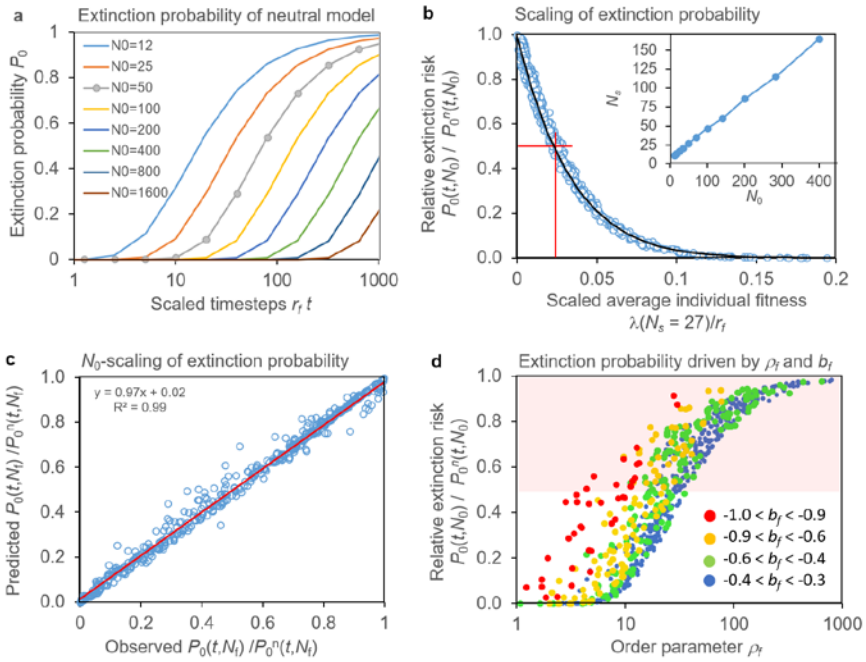

Figure 2. The scaling of the probability of extinction. a, The extinction probability $P_0^n(t, N_0)$ of the neutral model (equation 2a) for different initial conditions N_0, plotted over the scaled timestep $r_f\,t$. The grey dots highlight the case of initially $N_0 = 50$ individuals of scenario 1. **b**, Scale collapse of the extinction probability $P_0(t, N_0)$ for timestep $t = 200$ and $N_0 = 50$ by plotting the relative extinction probability $P_0\,(t, N_0)/P_0^n(t, N_0)$ over $\tilde{\lambda}_f(N_s = 27)/r_f$ where N_s is a suitable abundance and r_f the reproduction rate. The small inset shows how N_s depends on N_0 ($N_0 \approx 7 + 0.4\,N_s$). The red line indicates the threshold of $\tilde{\lambda}_f/r_f < 0.5$ associated with near-neutral behaviour and the black line is the fit with equation 17. **c**, Predicting the relative extinction risk for initial abundances $N_0 = N_f$ (x-axis), being the observed species abundances, based on the scaling of the relative extinction for initial abundances $N_0 = 50$ with equation 2b (y-axis). The red line is the 1-to-1 line. **d**, The the relative extinction probability, plotted for different values of the exponent b_f of the aggregation-abundance relationship (different colours) over the order parameter quantity $\rho_f = (J/N_f^*)\,B_f\,k_{fh}/(k_{ff} - k_{fh})$ (equation 15b). The red shaded area indicates near-neutral species with $\tilde{\lambda}_f(N_s = 27)/r_f < 0.025$, a threshold taken from b. The data are from scenario 1 (no niche differences, $N_0 = 50$).

We find that the parameterized birth-death model captures the full range of stochasticity incorporated into a symmetric (i.e., all species have the same parameters) individual-based implementation of our model, and is able to correctly predict the species abundance distribution of the individual-based simulations, given the same initial condition and the same number of simulation years are used (Extended Data Fig. 4). This is an important finding that links individual-based and analytical approaches and re-emphasizes the capacity of birth-death models to produce accurate species abundance distributions (Hubbell 2001; Azaele et al. 2006).

A "scale collapse" of the results of the birth-death model reveals, with unexpected clarity, the conditions under which a species can recover from low abundances. We find that the relative extinction probability $P_0(t, N_0)/P_0^n(t, N_0)$ for small

initial abundance (e.g., N_0 = 50) follows a function of the form $y(x) = (1 - x/x_0)^e$ of the scaled average individual fitness $\tilde{\lambda}_f(N_s)/r_f$, taken at a suitable abundance N_s (Fig. 2B), where the parameters N_s, e and x_0 depend on N_0 with $N_s(50) = 27$, $e(50) = 10$ and $x_0(50) = 0.35$ (see methods, equation 17). For values smaller or larger than N_s the relationship becomes blurred (Extended Data Fig. 5). Given the general difficulties to mathematically derive the full extinction probability $P_0(t, N_0)$ for birth-death models, this is an unexpected result that provides a direct and quantitative connection between the extinction risk and both, individual-level parameters and measures of spatial patterns, as incorporated into our mathematical model (equation 9).

To complete the scaling relationships, we show how the relative extinction probabilities for two different initial conditions are related to each other. We scale the relative extinction probability from a fixed (small) initial condition (i.e., N_0 = 50) to predict that of a variable initial condition N_0 (i.e., the observed species abundance N_f) by the scaling

$$\frac{P_0(t,N_0)}{P_0^n(t,N_0)} = \left(\frac{P_0(t,50)}{P_0^n(t,50)}\right)^{f(N_0/50)} . \qquad (2b)$$

where the function in the exponent approximates $f(N_0/50) \approx 0.29(N_0/50) + 0.71$ (Fig. 2C; Extended Data Fig. 6). The three key elements of our theory (i.e., equation 2a, Fig. 2B and equation 17, and equation 2b) allow us now to derive quantitative expectations of how the (spatial) mechanisms of our model impact the local extinction risk in species-rich communities.

Applying our theory to the 720 selected species of 21 ForestGEO plots (with diameter at breast height (dbh) > 10cm, $N_f \geq 50$, and $k_{ff} > k_{fh}$; see methods), we find that coexistence at all latitudes generally benefits from the negative density dependence arising from neighbourhood crowding (Fig. 3A, B). Because coexistence requires that specie at low abundances tend to increase (Chesson 2000), we investigated the local extinction probability for the 720 species when starting with a low number of individuals (i.e., N_0 = 50). We find that the stabilizing effect of pure neighbourhood crowding (i.e., con- and heterospecifics compete equally) reduces in this case the extinction risk for tropical, subtropical and temperate forests on average by factors 0.57, 0.52, and 0.38, respectively, with a clear latitudinal gradient (Fig. 3A). The proportion of species that behave near-neutrally declines substantially with latitude (Fig. 3B). When starting with N_0 = 50 individuals, 59% of the species investigated show within 1000 years an extinction risk smaller than 5% (Fig. 3C). When starting with the observed abundances (i.e., $N_0 = N_f^*$) this figure increases to 92%, and the proportion of near-neutrally species declines again substantially with latitude (Extended Data Fig. 7).

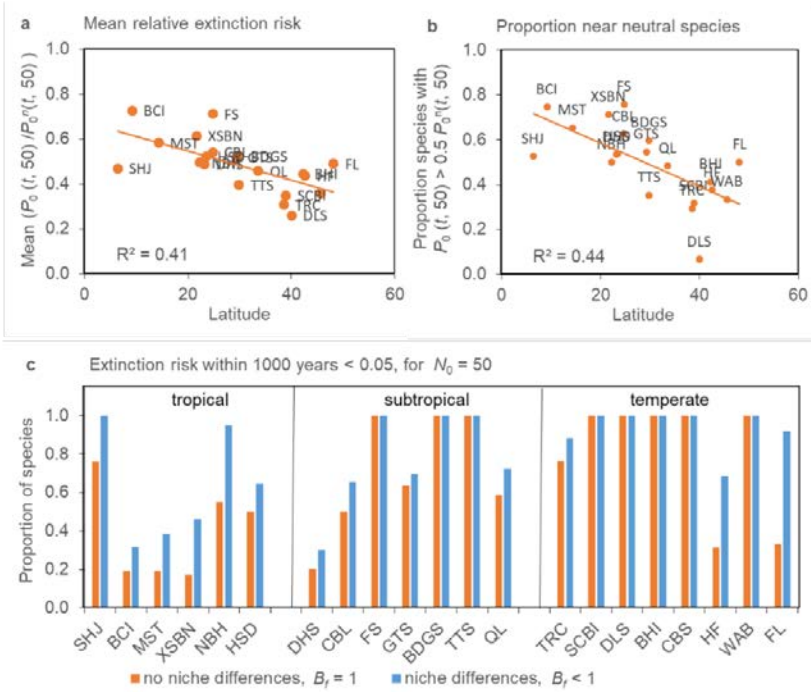

Figure 3. Reinterpretation of the invasion criterion to consider demographic stochsticity. We start each species with N_0 = 50 individuals, all other species are assumed to be quasi-stationary, and we used the birth-death model (equations 12, 13) parameterized for 720 species of the 21 ForestGEO plots to estimate the probability $P_0(t, 50)$ of local extinction after t = 200 timesteps (1000 years). **a,** Geographic variation in the mean reduction of the extinction probability due to the spatial crowding mechanism for scenario 1 (where con- and heterospecifics compete equally) relative to the corresponding neutral model (eq. 2a). **b**, Geographic variation in the proportion of species that behave near-neutral for scenario 1 (i.e., $P_0(t,50)/P_0^n(t,50) > 0.5$). **c**, The proportion of species with $P_0(t$ = 1000 yrs, N_0 = 50) < 0.05, estimated with the birth-death process (equations 12, 13). Orange: scenario 1 (i.e., B_f = 1), and blue: scenario 2 where we approximate niche differences by phylogenetic dissimilarity (i.e., B_f < 1). We excluded the temperate forest at CBS in panels A) and B) because the power law exponent < −1 produced an extinction risk higher than the neutral model (Extended Data Fig. 1C). We also excluded 15 species because they showed $k_{ff} < k_{fh}$.

Contrary to our expectation, we find a tendency of forests at lower latitudes to benefit less from the spatial coexistence mechanism (Figs. 3A, B, Extended Data Fig. 8). This is because the extinction risk is driven in our model by three main factors (equations 9, 14). The first factor, the exponent of the aggregation-abundance relationship (Fig. 1; Extended Data Fig. 1) favours tropical forests, but is overpowered by the quantity ρ (equations 14, 15b; Figure 2d; Extended Data Fig. 8A-C, E), which is dominated by the relative species abundances N_f^*/J that are generally lower at lower latitudes (Extended Data Fig. 8D), and the reproduction rate r_f (eq. 9a) that is generally lower at higher latitudes (Supplementary Table 1).

Using an expanded model version, we assess how the potential effects of niche differences may contribute to coexistence in our forest dynamics plots. For example, the proportion of species at low abundances (i.e., $N_0 = 50$) that showed a local extinction probability larger than 5% within 1000 years was on average 40% when assuming that con- and heterospecifics compete equally (scenario 1), but only 26% when assuming niche differences (scenario 2; Fig. 3C). We also found that the mean relative extinction probability was 0.52 for the case without niche differences (Fig. 3A) and 0.37 when assuming niche differences (Extended Data Fig. 9A), which is an additional reduction in the extinction probability by factor 0.71.

Discussion

Deriving a theory that integrates observed spatial patterns in forests with multiple ecological processes into mathematical theory is a formidable challenge. Here we have presented a unified theoretical framework that integrates stochastic models of birth-death processes with mathematical models of forest dynamics that links the effects of crowding competition mechanistically to spatial patterns at the scale of individual trees. Our theory provides a direct quantitative connection between the local extinction risk of a species and measures of spatial patterns, demographic parameters, mean niche overlap, and its relative abundance (Figure 2; equations 9, 14, 17, 18).

Several important ecological insights result from this new theory. First, it shows that coexistence at all latitudes generally benefits from the observed spatial patterns that drive neighbourhood crowding competition, and importantly, parameterizing the local extinction risk of small populations with the detailed spatial information provided by 21 ForestGEO plots, ranging from temperate to tropical, indicates that spatial mechanisms alone can account for coexistence of the majority of the 720 species analysed over a period of 1000 years at a local scale (Extended Data Fig. 7). This is an astonishing result, given that our mathematical model describes community dynamics in (smaller) forest plots without immigration, and without several of the processes that may additionally promote coexistence in species rich forests (e.g., Chesson 2000; Wright 2002; Usinowicz et al. 2017). We therefore expect that the extinction risk will further decline when assuming realistic immigration rates (Condit et al. 2012). However, while our estimates are conservative in this respect, our model does not include mechanisms such as environmental stochasticity (Lande 1993; Chisholm et al. 2014) that can increase the local extinction risk. We demonstrated here the power of our theoretical framework for a relatively simple example based on crowding competition impacting survival, but our

approach can be applied more generally to include additional mechanisms, as long as the average individual fitness can be translated into birth and death rates.

Second, our comprehensive analysis reveals an intriguing latitudinal gradient in the strength of the relationship between conspecific aggregation and abundance, with forests at lower latitudes tending to show weaker negative relationships, which suggest operation of stronger stabilizing negative frequency-dependency at tropical forests compared to temperate forests. However, our mathematical analysis showed that conspecific spatial aggregation is related in more complex ways with species coexistence since the local extinction probability of species depends additionally on the reproduction rate and an order parameter ρ_f (equation 14; Extended Data Fig. 8), which is driven by the relative species abundances (which are generally higher at larger latitudes). As a consequence, species coexisting at larger latitudes benefitted more from the stabilizing spatial mechanism than forests at lower latitudes (Fig. 3, Extended Data Fig. 7, 9). This reflects results from stochastic models that showed that the mean extinction time under demographic stochasticity increases nearly exponentially with the equilibrium population size (Lande 1993). However, for species with similar values of the order parameter ρ_f, the weaker negative frequency dependency caused by the negative aggregation-abundance relationship makes a difference (Figure 2d, Extended Data Fig. 8D-F) and leads to a higher extinction risk of low abundance species. This effect may contribute to the low number of less abundant species in temperate forests.

Third, current deterministic coexistence theory relies mostly on the deterministic invasion criterion (Chesson 2000), but we found that it was satisfied for nearly all forests analysed here (equation 10). It is therefore an unreliable predictor of species coexistence, given that cannot detect more subtle differences in the extinction risk of species related to demographic stochasticity (Schreiber et al. 2022; Shoemaker et al. 2020). However, our analysis revealed that the average individual fitness of small population sizes, which forms the basis of the deterministic invasion criterion, is directly related with the extinction risk of small populations via our equation 17 (Figure 2B). Thus, our stochastic invasion criterion naturally extends the deterministic invasion criterion to a probabilistic invasion criterion quantifying the risk of extinction. This allows us to assess how much the (spatial) coexistence mechanisms reduce the local extinction probability compared to that of the corresponding neutral model where the (spatial) mechanisms are absent, and what properties allow species to increase if at low abundances. We find that the order parameter $\rho_f = (J/N_f^*)B_f k_{fh}/(k_{ff} - k_{fh})$ (equation 14) dominates the value of the average individual fitness (Figure 2d, Extended Data Fig. 8A-F) and therefore measures the degree of stabilization incorporated into the model, with lower values indicating stronger stabilization and lower extinction risk. Thus, a species with low extinction

risk will typically show high aggregation k_{ff}, high abundance N_f^*, low values of B_f (i.e., larger niche differences), and low values of k_{fh} (i.e., strong segregation).

Our theory clarifies how the multiple interacting processes, including crowding competition, reproduction, niche overlap, alter together with emerging spatial patterns and the scaling of aggregation with abundance the predictions of the neutral model with respect to the extinction probability. However, what is less known is how species traits determine the values of the emerging spatial patterns (e.g., McFadden et al. 2019) and the abundance-aggregation relationship. Previous work (Wiegand et al. 2021) demonstrates that placement of most offspring close to their parents (i.e., dispersal limitation) is a powerful mechanism to generate negative aggregation-abundance relationships with coefficients close to –1, as observed here in temperate forests, and that weak negative aggregation-abundance relationships (i.e., coefficients close to zero), as observed for example at the BCI and Mo Singto forests (Fig. 1) that host a high diversity of animal seed dispersers, can be obtained if offspring is placed in clumps but largely independent of parent locations (on scales of tens of hectares; Wiegand et al. 2021). Indeed, biological evidence suggests that most species show some degree of dispersal limitation (Hubbell 2006), but that offspring may show additional clumping caused for example by animal seed dispersal, canopy gaps or edaphic habitat conditions (e.g., Muller-Landau et al. 2008; Wright et al. 2016; Masaki et al. 2019), which can account for clumping of offspring independent on parent locations. A second potential mechanism to generate a negative abundance-aggregation relationships is shared habitat filtering of different life stages (Kraft et al. 2015). When dispersal is short range, populations can build up in favourable locations due to an emerging positive fitness-density covariance (Chesson 2009). Note that our data analysis already includes the effect of habitat filtering in the measures k_{ff} and k_{fh} of spatial patterns. However, estimation of the magnitude of the fitness-density covariance for our data sets would require a species-specific parameterization of habitat-dependent survival rates.

Overcoming the limitations of phenomenological models as often used in contemporary coexistence theory (e.g., Chesson 2000; Allesina and Tang 2012; Kraft et al. 2015; Barbier et al. 2018; Serván et al. 2018; Stone 2018; Gibbs et al. 2022) require approaches that explicitly consider the lower-level processes that generated the phenomenon of interest (Loreau 2010). Our results demonstrate the utility of this approach by establishing “transfer functions” that capture spatial effects of local crowding competition at the microscale of individual plants, here described by commonly used individual-based neighbourhood crowding indices (Uriarte et al. 2004; Lasky et al. 2014; Wiegand et al. 2017; Fortunel et al. 2018), and transfer them as measures of spatial patterns into phenomenological models. This approach has the decisive advantage that the lower-level parameters of the transfer functions

can be parameterized from empirical or experimental knowledge, such as the ForestGEO data sets in our case. Taking this approach, we demonstrate that spatially-enhanced theoretical models that use the information on the emerging spatial neighbourhood patterns can explain coexistence of a high proportion of the species in our species rich forest plots. This finding has important consequences for ecological theory because it shows that spatial patterns can lead to coexistence of multiple species and emphasizes the need to understand the mechanisms underpinning their emergence in greater detail than has previously been appreciated.

References

Allesina, S. & Levine, J. M. A competitive network theory of species diversity. *Proc. Natl Acad. Sci. USA* **108**, 5638–5642 (2011).

Allesina, S. & Tang, S. Stability criteria for complex ecosystems. *Nature* **483,** 205–208 (2012).

Azaele, S., Pigolotti, S., Banavar J. R. & Maritan, A. Dynamical evolution of ecosystems. *Nature* **444**, 926–928 (2006).

Bailey, N. T. J. T*he Elements of Stochastic Processes with Applications to the Natural Sciences* (Wiley, 1964).

Barabás, G., D'Andrea, R. & Stump, S. M. Chesson's coexistence theory. *Ecol. Monogr.* **88,** 277-230 (2018).

Bleher, B., Oberrath, R. Böhning-Gaese, K. Seed dispersal, breeding system, tree density and the spatial pattern of trees: a simulation approach. *Basic and Applied Ecology* **3**, 115–123 (2002).

Canham, C. D., LePage, P. T., K. D. Coates. A spatially-explicit analysis of canopy tree competition: effects of shading versus crowding. *Canadian Journal of Forest Research* **34**, 778–787 (2004).

Chanthorn, W., Getzin, S., Wiegand, T., Brockelman, W. Y., and Nathalang, A. Spatial patterns of local species richness reveal importance of frugivores for tropical forest diversity. *J. Ecol.* **106,** 925–935 (2018).

Chesson, P. Mechanisms of maintenance of species diversity. *Annu. Rev. Ecol. Syst.* **31,** 343–366 (2000).

Chesson, P. Scale transition theory with special reference to species coexistence in a variable environment. *J. Biol. Dynamics* (2009).

Chesson, P. Scale transition theory: Its aims, motivations and predictions. *Ecol. Complex.* **10,** 52-68 (2012).

Chisholm, R. A. et al.; Temporal variability of forest communities: empirical estimates of population change in 4000 tree species. *Ecology Letters* **17**, 855–865 (2014).

Condit, R. et al. Spatial patterns in the distribution of tropical tree species. *Science* **288**, 1414–1418 (2000).

Connell, J. H. Diversity in tropical rain forests and coral reefs. *Science* **199**, 1302–1310 (1978).

Davies, S. J. et al. ForestGEO: Understanding forest diversity and dynamics through a global observatory network. *Biol. Conserv.* **253**, 108907 (2021).

Detto, M, and Muller-Landau, H. C. Stabilization of species coexistence in spatial models through the aggregation–segregation effect generated by local dispersal and nonspecific local interactions. *Theor. Pop. Biol.* **112**, 97–108 (2016).

Ellner, S.P., R.E. Snyder, P.B. Adler, and G. Hooker. Toward a “modern coexistence theory” for the discrete and spatial. *Ecol. Monogr.* **92**, e1548 (2022).

Flügge, A.J., Olhede, S.C. & Murrell, D.J. The memory of spatial patterns: changes in local abundance and aggregation in a tropical forest. *Ecology* **93**, 1540–1549 (2012).

Fortunel, C., Valencia, R., Wright, S. J., Garwood, N. C. & Kraft, N. J. B. Functional trait differences influence neighbourhood interactions in a hyperdiverse Amazonian forest. *Ecol. Lett.* **19,** 1062–70 (2016).

Getzin, S., Wiegand, T., Wiegand, K. & He, F.. Heterogeneity influences spatial patterns and demographics in forest stands. *J. Ecol.* **96**, 807–820. (2008).

Gibbs T., Levin S. A. & Levine J. M. Coexistence in diverse communities with higher-order interactions. *Proc. Natl Acad. Sci. USA* **119**, e2205063119 (2022).

Grimm, V. & C. Wissel. The intrinsic mean time to extinction: a unifying approach to analysing persistence and viability of populations. *Oikos* **105**, 501–511 (2004).

He, F., & Duncan, R. P. Density-dependent effects on tree survival in an old-growth Douglas fir forest. *J. Ecol.* **88**, 676–688 (2000).

He, F., Legendre, P., LaFrankie, J.V. Distribution patterns of tree species in a Malaysian tropical rain forest. J. Veg. Sci. **8**, 105-114 (1997).

Hubbell, S. P. Tree dispersion, abundance, and diversity in a tropical dry forest. *Science* **203**, 1299–1309 (1979).

Hubbell, S. P. *The Unified Neutral Theory of Biodiversity and Biogeography*. (Princeton Univ. Press, 2001).

Hubbell, S. P. Neutral theory and the evolution of functional equivalence. *Ecology* **87,** 1387–1398 (2006).

Janzen 1970; Janzen, D. H. Herbivores and the number of tree species in tropical forests. *Am. Nat.* **104**, 501–528 (1970).

Klausmeier, C.A, & Tilman, D. Spatial models of competition. In *Competition and Coexistence* (eds. Sommer, U. & Worm, B.) pp 43–78 (Springer, 2002).

Kraft, N. J. B., Godoy, O. & Levine, J. M. Plant functional traits and the multidimensional nature of species coexistence. *Proc. Natl Acad. Sci. USA* **112,** 797–802 (2015).

Lande, R. Risks of population extinction from demographic and environmental stochasticity and random catastrophes. *Am. Nat.* **142**, 911–927 (1993).

Lasky, J. R., Uriarte, M., Boukili, V. K., & Chazdon, R.L. Trait-mediated assembly processes predict successional changes in community diversity of tropical forests. *Proc. Natl Acad. Sci. USA* **111**, 5616–21 (2014).

Levine, J. M., Bascompte, J., Adler, P. B. & Allesina, S. Beyond pairwise mechanisms of species coexistence in complex communities. *Nature* **546**, 56–64 (2017).

Lewis, S. L. & Tanner, E. V. J. Effects of above- and belowground competition on growth and survival of rain forest tree seedlings. *Ecology* **81**, 2525–2538 (2000).

Loreau, M. *From Populations to Ecosystems.* (Princeton Univ. Press, 2010)

Mangan, S. A. et al. Negative plant–soil feedback predicts tree-species relative abundance in a tropical forest. *Nature* **466**, 752–755 (2010).

Masaki, T. et al. Impact of the spatial uncertainty of seed dispersal on tree colonization dynamics in a temperate forest. *Oikos* **128**, 1816–1828 (2019).

May, F., Wiegand, T. Lehmann, S. & Huth A. Do abundance distributions and species aggregation correctly predict macroecological biodiversity patterns in tropical forests? *Glob. Ecol. Biogeogr.* **25,** 575–585 (2016).

McFadden, I. R. et al. Disentangling the functional trait correlates of spatial aggregation in tropical forest trees. *Ecology* **100**, e02591 (2019).

Muller-Landau, H. C. et al. Interspecific variation in primary seed dispersal in a tropical forest. *J. Ecol.* **96**, 653–667 (2008).

Plotkin, J.B., et al. Species-area curves, spatial aggregation, and habitat specialization in tropical forests. *J. Theor. Biol.* **207**, 81–99 (2000).

Réjou-Méchain, M. et al. Spatial aggregation of tropical trees at multiple spatial scales. J. *Ecol.* **99**, 1373–1381 (2011).

Schreiber, S. J. et al. Does deterministic coexistence theory matter in a finite world? *Ecology*, **104**, e3838 (2022).

Seidler, T. G., & Plotkin, J. B. Seed dispersal and spatial pattern in tropical trees. *PLoS Biology* **4**, e344 (2006).

Serván, C. A., Capitán, J. A., Grilli, J., Morrison, K. E. & Allesina, S. Coexistence of many species in random ecosystems. *Nat. Ecol. Evol.* **2,** 1237–1242 (2018).

Shoemaker, L. et al. Integrating the underlying structure of stochasticity into community ecology. *Ecology* **101,** e02922 (2020).

Sterner, R. W. et al. Testing for life historical changes in spatial patterns of four tropical tree species. *J. Ecol.* **74**: 621–633 (1986).

Stone, L. The feasibility and stability of large complex biological networks: a random matrix approach. *Sci. Rep.* **8,** 8246 (2018).

Uriarte M., Canham, C. D., Thompson, J., & Zimmerman, J. K. Understanding natural disturbance and human land use as determinants of tree community dynamics in a subtropical wet forest: results from a forest simulator. *Ecol. Monogr.* **79**, 423–43 (2009).

Uriarte, M., *et al.* Trait similarity, shared ancestry and the structure of neighbourhood interactions in a subtropical wet forest: implications for community assembly. *Ecol. Lett.* **13,** 1503–1514 (2010).

Usinowicz, J., *et al.* Temporal coexistence mechanisms contribute to the latitudinal gradient in forest diversity. *Nature* **550,** 105–108 (2017).

Wiegand, T., *et al.* Spatially explicit metrics of species diversity, functional diversity, and phylogenetic diversity: insights into plant community assembly processes. *Annu. Rev. Ecol. Syst.* **48,** 329–351 (2017).

Wiegand, T. et al. Consequences of spatial patterns for coexistence in species-rich plant communities. *Nat. Ecol. Evol.* **5**, 965–973 (2021).

Wright, J. S. Plant diversity in tropical forests: a review of mechanisms of species coexistence. *Oecologia* **130,** 1–14 (2002).

Wright, J. S. et al. Interspecific associations in seed arrival and seedling recruitment in a Neotropical forest. *Ecology* **97**, 2780–2790 (2016).

Methods

Study areas

Twenty-one large forest dynamics plots of areas between 20 and 50 ha were utilized in the present study (Supplementary Table 1). The forest plots are part of the Forest Global Earth Observatory (ForestGEO) network (Davis et al. 2021) and are located in Asia and the Americas ranging in latitudes from 6.40° N to 48.08° N. Tree species richness among these plots ranges from 36 to 468. All free-standing individuals with diameter at breast height (dbh) ≥1 cm were mapped, size measured, and identified. We focussed our analysis here on individuals with dbh ≥ 10 cm (resulting in 313,434 individuals) and tree species with more than 50 individuals (resulting in initially 737 species). The 10 cm size threshold excludes most of the saplings and enables comparisons with previous spatial analyses. For 17 of our 21 plots, we obtained data on the mortality rate of trees with dbh ≥ 10 cm within a 5 year census interval (Supplementary Table 1) and by assuming approximate equilibrium we used this value in our model for the reproduction rate r_f (for all others plots we used the value of $r_f = 0.1$). We could estimate the mortality rate for each plot only for all species together, but not for individual species. However, the scaling of the extinction risk with reproduction rate (Fig. 2B, equation 2a) allows for assessment of the effects of variability in species-specific rates.

Shrub species were excluded. We also excluded 15 species because they showed lower levels of aggregation than segregation (i.e., $k_{ff} < k_{fh}$; Box 1), ten of them from BCI, two from MST, two from NBH, and one from FS. These (generally less abundant) species are probable relicts of an earlier successional episode when the species was once more abundant (Hubbell 1979; Flügge et al. 2012). We also excluded the two species *Picea mariana* and *Thuja occidentalis* of the Wabikin forest that are located in a patch of successional forest that was logged approximately 40 years ago (Wang et al. 2013).

Proxy for pairwise competition strength between species

Some of our analyses require the ratio β_{fj}/β_{ff} (Box 1) that describes the relative competitive effect (Uriarte et al. 2010) of individuals of species *i* on an individual of the focal species *f*. In general, it is difficult to derive estimates for the pairwise interaction coefficients β_{fj} (Canham et al. 2006) because this would require unfeasible large data sets to obtain a sufficient number of neighboured *f–j* species pairs for less abundant species. We therefore compare two scenarios for the ratio β_{fj}/β_{ff}. In scenario 1 we assume that con- and heterospecifics compete equally, thus $\beta_{fj} = \beta_{ff}$. In an analysis of sapling survival at BCI using NCI's, this scenario was the most parsimonious model for the majority of species (Uriarte et al. 2005) and represents

the extreme case without stabilizing niche overlap. In scenario 2 we assume that close relatives compete more strongly or share more pests than distant relatives (Fortunel et al. 2016). As proxy for this effect, we used phylogenetic distances (Erickson et al. 2014), given in millions of years (MA), as a surrogate for the relative competition because they are available for the species in our plots based on molecular data and the Phylomatic informatics tool (Webb and Donoghue 2005). In this we assume that functional traits are phylogenetically conserved (Uriarte et al. 2010; Fortunel et al. 2016; Cadotte et al. 2017). To obtain consistent measures among forest plots, phylogenetic similarities were scaled between 0 and 1, with conspecifics set to 1 and a similarity of 0 was assumed for a phylogenetic distance of 1200 MA, which was somewhat larger than the maximal observed distance (1059 MA). This was necessary to avoid discounting crowding effects from the most distantly related neighbours (Fortunel et al. 2016).

Crowding indices and measures of spatial patterns

We use a minimal spatially-explicit mathematical model to study the consequences of neighbourhood crowding on community dynamics and the local risk of extinction of small tree populations. The model assumes that survival of a focal tree k is reduced in areas of high local density of con- and heterospecifics (i.e., neighbourhood crowding), e.g., through competition for space, light or nutrients, or natural enemies (Janzen 1970; Connell 1971; Lewis et al. 2000; Mangan et al. 2010), while reproduction is density-independent with per capita rate r_f.

We describe the neighbourhood crowding around tree k of a focal species f by commonly used "neighbourhood crowding indices" (*NCI*'s; Uriarte et al. 2004; Box 1), but use separate indices for con- and heterospecific trees. The conspecific crowding index C_{kf} counts the number of conspecific neighbours j of species f that have a distance d_{kj} smaller than the neighbourhood radius r, but weights them by $1/d_{kj}$, assuming that farther away neighbours compete less (equation 3a). The crowding index H_{kf} does the same with all heterospecifics (equation 3b), and the crowding index I_{kf} weights heterospecifics additionally by their relative competitive effect β_{fj}/β_{ff} (equation 3c). Thus, we have

$$C_{kf} = \sum_{j=1}^{n_f} \frac{1}{d_{kj}} \tag{3a}$$

$$H_{kf} = \sum_{i \neq f} \sum_{j=1}^{n_i} \frac{1}{d_{kj}} \tag{3b}$$

$$I_{kf} = \sum_{i \neq f} \sum_{j=1}^{n_i} \frac{\beta_{fi}}{\beta_{ff}} \frac{1}{d_{kj}} \tag{3c}$$

where n_i is the total number of neighbours of species i within distance r of the focal individual, d_{kj} is the distance between the focal individual k and its jth neighbour of species i, and β_{fi}/β_{ff} is the competitive effect of one individual of species i relative to that of the focal species f (Uriarte et al. 2004; Lasky et al. 2014; Wiegand et al. 2017; Fortunel et al. 2018).

To link the survival of an individual k to its crowding indices we assume that the survival rate s_{kf} of a focal tree k of species f is then given by

$$s_{kf} = s_f \, exp(- \beta_{ff} \, (C_{kf} + I_{kf})), \tag{4}$$

where s_f is a density-independent background survival rate of species f and β_{ff} the individual-level conspecific interaction coefficients of species f (Uriarte et al. 2004). Statistical analyses with neighbourhood crowding indices have shown that the performance of trees depends on their neighbours for r between 10 and 15 m, we therefore estimate all measures of spatial neighbourhood patterns with a neighbourhood radius of r = 15 m. We investigate two scenarios, in scenario 1 con- and heterospecifics competing equally at the individual scale (i.e., $\beta_{fi} = \beta_{ff}$), and in scenario 2 the quantity β_{fi}/β_{ff} is proportional to phylogenetic similarity see above "*Proxy for pairwise competition strength between species*").

We use scale transition theory (Chesson 2009, 2012) and spatial point process theory (Wiegand and Moloney 2014) to transfer the individual-based "microscale" information on the number and distance of con- and heterospecific neighbours of focal individuals, which are provided by the ForestGEO census maps, into "macroscale" models of community dynamics without immigration (Wiegand et al. 2021). The average population-level survival rate $\bar{s}_f$ is given by

$$\bar{s}_f = s_f exp(-\beta_{ff}(\gamma_{ff}\overline{C_{kf}} + \gamma_{f\beta}\overline{I_{kf}})) \tag{5}$$

where the quantities γ_{ff} and $\gamma_{f\beta}$ capture the effects of non-linearity through the negative exponential relationship between survival and crowding, but in our case of high survival they can be neglected (i.e., $\gamma_{ff} \approx 1$ and $\gamma_{f\beta} \approx 1$) (Wiegand et al. 2021). The averages of the crowding indices can be decomposed into measures of spatial patterns and abundances

$$C_{ff} \equiv \overline{C_{kf}} = c \, k_{ff} N_f \tag{6a}$$

$$H_{fh} \equiv \overline{H_{kf}} = c \, k_{fh} \textstyle\sum_{i \neq f} N_i \tag{6b}$$

$$I_{fh} \equiv \overline{I_{kf}} = H_{fh} \frac{I_{fh}}{H_{fh}} = (c \, k_{fh} \textstyle\sum_{i \neq f} N_i) \, B_f \approx \; c \, k_{fh} B_f (J - N_f) \tag{6c}$$

where $c = 2\pi r/A$ is a scaling factor, A the area of the plot, r the radius of the neighbourhood, k_{ff} is a measure of the conspecific pattern of species f (with values of $k_{ff} > 1$ indicating aggregation, $k_{ff} < 1$ regularity and $k_{ff} = 1$ random patterns), k_{fh} is a measure of the placement of heterospecifics in the neighbourhood of the species f (with values of $k_{fh} < 1$ indicating segregation, $k_{fh} > 1$ attraction and $k_{fh} = 1$ independent placement), $B_f = I_{fh}/H_{fh}$ describes the effect of niche differences (i.e., the average reduction in the competition strength of heterospecifics compared to conspecifics), and J is the total number of individuals in the plot.

Equation (6c) uses two findings of earlier work (Wiegand et al. 2021). First, the quantity $B_f = I_{fh}/H_{fh}$ that summarizes the emerging effects of the individual-level interaction coefficients β_{fi}/β_{ff} at the population-level is for species rich forests at or near a stationary state in good approximation a species-specific constant (see Supplementary Text in Wiegand et al. 2021), suggesting diffuse neighbourhood competition where the competition strength of a heterospecific is on average factor B_f lower than that of conspecifics. Second, local density dependence leads in species rich forests at or near a stationary state to zero-sum dynamics (Hubbell 2001) with approximately J individuals. These approximations summarized in equation 6c decouple the multispecies dynamics and allows us to investigate the dynamics of individual species in good approximation.

In figure 1 we fitted for the species of a given forest plot a phenomenological power law where the x-value was the abundance N_f of the species and the y-value the corresponding aggregation k_{ff}. However, this leads for large abundances to values of k_{ff} close to zero, which are not in agreement with our data. Instead, the lowest possible value of the summary function k_{ff} under crowding competition is given by the value of heterospecific segregation k_{fh} if con- and heterospecifics compete equally. Thus, to avoid a bias we fit a power law using abundance N_f as the x-value and the quantity $k_{ff} - k_{fh}$ as y-value.

Basic community-level model

Combining equations (1), (5) and (6) leads to the general macroscale model based on the average individual fitness $\tilde{\lambda}_f(N_{f,t})$:

$$\frac{N_{f,t+1}-N_{f,t}}{\Delta t}\frac{1}{N_{f,t}} = \tilde{\lambda}_f(N_{f,t}) = (r_f - 1) + s_f exp(-\beta_{ff} W_f(N_{f,t})) \qquad (7a)$$

that describes the abundance $N_{f,t}$ of species f at timestep t using the "fitness factor"

$$W_f(N_{f,t}) = c\{k_{ff}N_{f,t} + B_f k_{fh}(J - N_{f,t})\}, \qquad (7b)$$

which we rewrite to accommodate the power law in $(k_{ff} - k_{fh})$ to:

$$W_f(N_{f,t}) = c\{(k_{ff} - k_{fh})N_{f,t} + k_{fh}(1 - B_f)\, N_{f,t} + B_f k_{fh} J\}. \qquad (7c)$$

To parameterize the model of equation (7), we use the ForestGEO data sets to determine the values of aggregation k_{ff}, segregation k_{fh}, total community size J, the observed abundance N_f^* of species f, the reproduction rate r_f, and the power law exponent b_f that describes the scaling of aggregation with abundance (equation 8). In all analyses we set the background survival rate to $s_f = 1$. With this setting we assume that all mortality is due to neighbourhood crowding. To determine the unknown value of β_{ff}, the individual-level conspecific interaction coefficients of species f, we assume that the observed species abundance N_f is close to equilibrium N_f^* and obtain from equation (7a) $\beta_{ff} = -\ln\left(\frac{1-r_f}{s_f}\right)/W_f(N_f^*)$.

To obtain the scaling of aggregation with abundance, we determined for each plot the exponent b_f of a power law, where abundance N_f was the x-value and the quantity $k_{ff} - k_{fh}$ the y-value. We then consider this scaling by replacing in equation (7b) the quantity $k_{ff} - k_{fh}$ by the power law

$$PL(N_f) = (k_{ff} - k_{fh})\,(N_f\,/\,N_f^*)^{b_f}. \qquad (8)$$

Note that $PL(N_f^*) = (k_{ff} - k_{fh})$. With equation (8) we obtain our final spatially-enriched model that links the macroscale to the microscale:

$$\frac{N_{f,t+1} - N_{f,t}}{\Delta t}\frac{1}{N_{f,t}} = \tilde{\lambda}_f(N_{f,t}) = (r_f - 1) + s_f\left(\frac{1-r_f}{s_f}\right)^{\frac{W_f(N_{f,t})}{W_f(N_f^*)}} \qquad (9a)$$

with $$W_f(N_{f,t}) = c\{PL(N_{f,t})\, N_{f,t} + (1 - B_f)k_{fh}N_{f,t} + B_f k_{fh} J\}. \qquad (9b)$$

The deterministic invasion criterion

Coexistence requires that populations at low abundances N_f increase, thus $\tilde{\lambda}_f(N_f) > 0$ (Chesson 2000). This is the case if $W_f(N_f)/W_f(N_f^*) < 1$ (equation 9a), which leads to the deterministic invasion criterion:

$$\left(\frac{N_f}{N_f^*}\right)^{b_f+1} < 1 + (1 - B_f)\frac{k_{fh}}{k_{ff} - k_{fh}}\left(1 - \frac{N_f}{N_f^*}\right) < 1 + (1 - B_f)\frac{k_{fh}}{k_{ff} - k_{fh}} \qquad (10)$$

and with $\kappa_f = (1 - B_f)\frac{k_{fh}}{k_{ff} - k_{fh}}$ and $N_f = 1$ we find the condition

$$b_f > -1 - ln(1 + \kappa_f)/\, ln(N_f^*) \qquad (11a)$$

In the case that con- and heterospecifics competing equally (i.e., $B_f = 1$) this reduces to:

$$b_f > -1 \tag{11b}$$

which is always fulfilled if the power law exponent satisfies $b_f > -1$. However, this criterion is somewhat unsatisfying because all forest plots, except the CBS plot, fulfil it. More importantly, the deterministic invasion criterion does not consider the detrimental influence of demographic stochasticity, which can produce a high risk of extinction at small population sizes, even if the average individual fitness $\tilde{\lambda}_f$ shows positive values. We therefore introduce in the next section a stochastic invasion criterion that considers the effect of demographic stochasticity.

In the case of niche differences (i.e., $B_f < 1$), equation (11a) indicates that the power law exponent b_f can even be the smaller than –1 if B_f is small, $k_{fh}/(k_{ff} - k_{fh})$ larger, or N_f^* smaller. Indeed, we find that a few species of the CBS plot, which shows a power law exponent of $b_f = -1.077$, fulfil the deterministic invasion criterion due to large values of $k_{fh}/(k_{ff} - k_{fh})$ (and $B_f < 1$; Extended Data Fig. 10). A power law with exponent $b_f < -1$ leads to a type of Allee effect, which reduces the growth rate at low abundances or makes it even negative, in the latter case causing a high extinction risk for small populations (for example, the species *Ulmus japonica* (acronym ULMJAP) shows an extinction risk of 87% within 1000 years) (Extended Data Fig. 10).

Considering demographic stochasticity

A small population may go extinct by random events due to demographic stochasticity even if the invasion criterion is satisfied (Schreiber et al. 2022). To introduce demographic stochasticity, we translate the average individual fitness $\tilde{\lambda}_f(N_f)$ into the master-equation framework of a Markov process of birth-death type, which allows for estimation of the probability distribution $P_0(t)$ that a species with initially N_0 individuals will be extinct at timestep t (Grimm and Wissel 2004). A convenient property of the birth-death model is that it uses deterministic equations to describe demographic stochasticity and does therefore not require stochastic simulations to determine extinction probabilities.

The birth-death model describes the dynamics of the probability distribution $P_n(\tau)$ at timestep τ by considering the probabilities b_n and d_n that one reproduction or one death event occurs in a very small timestep $\delta\tau$, respectively, if the population has n individuals. We find from equation (7a) that

birth rate: $b_n = n\ \delta\tau\ r_f$ (12a)

death rate: $d_n = n\ \delta\tau\ [1 - s_f\ exp(-\beta_{ff}\ W_f(n))]$ (12b)

$d_n = n\ \delta\tau\ r_f$ (12c)

Equation (12c) gives the death rate of the corresponding neutral birth-death model. We select a small timestep of $\delta\tau = \Delta t/4000$ in relation to the 5 year timestep Δt of the macroscale model to guarantee that the probabilities for one birth and death during $\delta\tau$ are well below one.

The birth-death model describes the dynamics of the probability distribution $P_n(\tau)$ and is given by

$$P_0(\tau + 1) = P_0(\tau) + d_1\ P_1(\tau) \quad (13a)$$

$$P_n(\tau + 1) = b_{n-1}\ P_{n-1}(\tau) + (1 - b_n - d_n)\ P_n(\tau) + d_{n+1}\ P_{n+1}(\tau) \quad (13b)$$

The first equation (13a) gives the extinction probability in the next timestep τ+1, it is the extinction probability $P_0(\tau)$ at the previous timestep τ plus the probability d_1 of one death event (for a population with abundance 1) times the probability $P_1(\tau)$ that the population had the previous timestep τ an abundance of $n = 1$. The second equation (equation 13b) is a book keeping of the different possibilities that either a birth event happens, no event happens, or a death event happens. A birth event means that a population of $n - 1$ individuals (with probability $P_{n-1}(\tau)$) gains one individual (with probability b_{n-1}), a death event means that a population of n +1 individuals (with probability $P_{n+1}(\tau)$) loses one individual (with probability d_{n+1}), and the population maintains n individual (with probability $P_n(\tau)$) if no birth or death event happens (with probability $1 - b_n - d_n$).

We iterated equation (13) in a straight-forward way using appropriate initial conditions $P_n(\tau = 0)$, which was either a value of $n = 50$ to represent a small population size for assessment of the invasion criterion ($n = 50$ is also the abundance threshold for populations to be included in our analysis), the observed species abundance, or the species abundance distribution resulting from individual-based simulations to test the birth-death model framework. Given that very high abundances n occur with extremely low probabilities $P_n(\tau)$, we defined a maximal abundance $n_{\max}$ above which we could safely set $P_n(\tau) = 0$ for $n > n_{\max}$. We used the small probability $P_n(\tau) < 10^{-9}$ as threshold value to determine $n_{\max}$, and we updated this value every 100 small timesteps $\delta\tau$. This adaptive scheme of a dynamic selection of $n_{\max}$ guarantees both, computational efficiency and fulfilment of the normalization condition $\sum_{n=0}^{n_{max}} P_n(\tau) = 1$.

Our results show that the extinction risk of small populations with N_f = 50 individuals depends critically on the ratio $W_f(N_f)/W_f(N^*_f)$ of the fitness factors given at equation (9b) (Fig. 2B). The ratio can be expressed as

$$\frac{W_f(N_f)}{W_f(N_f^*)} = \frac{(\frac{N_f}{N_f^*})^{b_f+1} + \kappa_f\,(\frac{N_f}{N_f^*}) + \rho_f}{1+\kappa_f+\rho_f} \tag{14}$$

with

$$\kappa_f = \left(1 - B_f\right)\frac{k_{fh}}{k_{ff}-k_{fh}} \tag{15a}$$

$$\rho_f = B_f\,\frac{k_{fh}}{k_{ff}-k_{fh}}\,\frac{J}{N_f^*}. \tag{15b}$$

For the case that con- and heterospecifics compete equally at the individual scale (i.e., B_f = 1) we obtain the simpler condition

$$\frac{W_f(N_f)}{W_f(N_f^*)} = \frac{(\frac{N_f}{N_f^*})^{b_f+1} + \rho_f}{1+\rho_f}, \tag{16}$$

with the two summands depending on two main factors, $(N_f/N_f^*)^{bf+1}$ introduced by the abundance-aggregation relationship with exponent b_f, and the order parameter ρ_f that largely drives the extinction risk (Figure 2d, Extended Data Fig. 8D-F), and which contains information on the ratio $k_{fh}(/k_{ff} - k_{fh})$ of segregation to aggregation and the relative species abundances N_f/J (Extended Data Fig. 8). Interestingly, the order parameter ρ_f drops out in the deterministic invasion criterion (see Supplementary Text).

Scaling of the relative extinction probability

The average individual fitness $\tilde{\lambda}_f(N_f)$ drives the dynamics of the expected population sizes (equation 7a), and we suspect that the relative extinction probability $P_0(t, N_0)/P_0{}^n(t, N_0)$ of the corresponding birth-death model (eq. 12), for small initial abundances N_0 and not too large time steps t, should be related to some indices of the values of $\tilde{\lambda}_f(N_s)$ for suitable abundance N_s somewhat below the initial abundance N_0. For larger timesteps t the influence of the initial conditions vanishes and $P_0(t, N_0)$ will approximate its quasi-stationary distribution, which is independent on the initial abundance. To identify suitable indices, we determined the extinction probability $P_0(t, N_0)$ for time step t = 200 and several initial conditions N_0, and tested indices including $\tilde{\lambda}_f(N_f)$ for different abundances N_f, the slopes $\frac{d\tilde{\lambda}_f(N_f)}{dN_f}\Big|_{N_f=0}$, $\frac{d\tilde{\lambda}_f(N_f)}{dN_f}\Big|_{N_f=N_0}$, $\frac{d\tilde{\lambda}_f(N_f)}{dN_f}\Big|_{N_f=N_f^*}$, and the sum $\sum_{N=1}^{N_0}\tilde{\lambda}_f(N)$.

To our surprise we found that the average individual fitness $\tilde{\lambda}_f(N_s)$, when taken at a suitable abundance N_s and divided by its maximal possible value r_f, fully determines the relative extinction probability (Fig. 2b). The scaling with the reproduction rate r_f is reasonable, since it basically scales the time step t. Extended Data Figure 5 shows one example for an initial condition $N_0 = 50$ and different values of N_s. By repeating this exercise for different smaller initial abundances N_0, ranging from 12 to 100, we found that the suitable abundance N_s can be approximated by $N_s(N_0) = 7 + 0.4\, N_0$.

The next task is to determine the functional form of the relationship shown in Figure 2b. We find that it approximates the simple function $f(x) = (1 - \frac{x}{\lambda_0})^e$ very well, where $x = \tilde{\lambda}_f(N_s)/r_f$ and λ_0 and e are parameters. The parameter λ_0 can be approximated as $\lambda_0(N_0) = 0.4 - N_0\ /870$ and the exponent e by $e(N_0) = N_0\ (0.24 - N_0/1233)$. In summary, we obtain for small initial abundances N_0 the empirical scaling of the relative extinction probability

$$\frac{P_0(t{=}200,N_0)}{P_0^n(t{=}200,N_0)} = \left(1 - \frac{\tilde{\lambda}_f(7+0.4N_0)}{(0.4-\frac{N_0}{870})}/r_f\right)^{N_0(0.24-\frac{N_0}{1233})} \tag{17}$$

Equation 17 describes the scaling of the relative extinction probability for small timesteps t and small initial abundances N_0 (say up to 100), but for larger values of N_0 some issues appear. For example, if the initial abundances N_0 is larger than the equilibrium N_f^* the extinction probability may actually be larger than that of the neutral model. This is because the average individual fitness $\tilde{\lambda}_f$ is negative for $N_f > N_f^*$, which reduces the abundance quicker on average than the respective neutral model where $\tilde{\lambda}_f$ is always zero. Additionally, the relationship become more blurred for larger initial abundances N_0.

We therefore develop a second scaling relationship to predict the relative extinction probability for larger initial abundances based on the relative extinction probability for small initial abundances that we can estimate with equation 17. Motivated by the scaling of the extinction probability of the neutral model with initial abundance N_0 (equation 2a), where each individual that is initially present initiates one independent Markov chain, we scale the relative extinction probability from a fixed initial condition (e.g., $N_0 = 50$) to a variable initial condition N_0 by

$$\frac{P_0(t,N_0)}{P_0^n(t,N_0)} = \left(\frac{P_0(t,50)}{P_0^n(t,50)}\right)^{f(N_0/50)}. \tag{18}$$

where the exponent is a function of the ratio of the two initial abundances $N_0/50$. We find that the simple function $f(N_0/50) \approx 0.29\ (N_0/50) + 0.71$ approximates the exponent well (Fig. 2C; Extended Data Fig. 6.

Scenarios investigated with the birth-death model

We conducted four experiments with the birth-death model to assess the effects of the spatial mechanism of neighbourhood crowding on the ability of species to persist for 1000 years when having low abundances (i.e., N_0 = 50; scenarios 1, 2), and to assess the extinction risk of the species within 1000 years at their current abundance (i.e., $N_0 = N_f$; scenarios 3 and 4). Scenarios 1 and 3 assumed that con- and heterospecifics compete equally (i.e., no niche differences; $\beta_{fi} = \beta_{ff}$, $B_f = 1$), and scenarios 3 and 4 consider niche differences between species approximated by phylogenetic dissimilarity. To this end we assumed that the individual-level interaction coefficients β_{fi} are proportionally to phylogenetic similarity (i.e., $\beta_{fi} < \beta_{ff}$, $B_f < 1$; see above "*Proxy for pairwise competition strength between species*"). We also conducted analyses with different initial conditions N_0 = 12, 18,25, 36, 50, 71, 100, 141, 200, 283, 400 to establish a relationship between N_0 and the suitable abundance N_S (Figure 2b) where the scaled average individual fitness $\tilde{\lambda}_f(N_s)/r_f$ shows the best relationship to the relative extinction probability $P_0(t, N_0)/P_0^n(t, N_0)$.

Parameterization of the simulation model

The simulation model used here is described in Wiegand et al. (2021) and the Supplementary Text. It is an individual-based and spatially explicit and stochastic implementation of the spatial multi-species model (equation 9). In contrast to Wiegand et al. (2021), we use here distance-weighting for the estimation of the crowding indices. Thus, in the source code (published as Supplementary information in Wiegand et al. 2021) we use now DistanceWeighting = 1 instead of DistanceWeighting = 0.

The simulations of the individual-based model were conducted over 5000 census periods in an area of A = 200 ha, and comprised approximately 86,000 trees with initially 80 species. There was no immigration. The model parameters were the same for all species, and all species followed exactly the same model rules. We selected $\beta_{fi} = \beta_{ff}$ to obtain no differences in con- and heterospecific interactions and s_f = 1 (no background mortality), and we adjusted the parameters β_{ff} = 0.02 and r_f = 0.1 to yield tree densities (430/ha) and an overall 5 year mortality rate (10%) similar to that of trees with dbh ≥ 10cm of the BCI plot (Wiegand et al. 2017). The radius of the neighbourhood used to estimate the crowding indices was r = 15m.

To test if the birth-death model is able to correctly predict the species abundance distribution of an individual-based implementation of our model, we applied the

individual-based model for three different parameterizations that produce typical average individual fitness functions (Extended Data Figure 4A). To this end we varied two key parameters of the model that influence the aggregation-abundance relationship. The first was the parameter σ of the Gaussian kernel that is used in the model to place recruits around conspecific adults or around random cluster. We used parameter values of σ = 67, 15, 10 m for our 3 simulation runs to produce one scenario with weak spatial aggregation (σ = 67) and two scenarios with smaller-scale aggregation (σ =15, 10 m) that mimic realistic seed dispersal distances. The second key parameter was the proportion p_d of recruits to be placed around randomly distributed cluster centres (the proportion 1− p_d is placed around randomly selected conspecific adults). We used parameter values of p_d = 0.0125, 0.6, and 1. The proportion of p_d of recruits of each species were placed around 16 randomly distributed cluster centres that changed every timestep their location.

Additional Method References

Cadotte, M. W., Davies, T. J. & Peres-Neto, P. R. Why phylogenies do not always predict ecological differences. *Ecological Monographs* **87,** 535–551 (2017).

Erickson, D. L. *et al.* Comparative evolutionary diversity and phylogenetic structure across multiple forest dynamics plots: a mega-phylogeny approach. *Front. Genet.* **5,** 358 (2014).

Fortunel, C., Lasky, J. R., Uriarte, M., Valencia, R., Wright, S. J., Garwood, N. C. & Kraft, N. J. B. Topography and neighborhood crowding can interact to shape species growth and distribution in a diverse Amazonian forest. *Ecology* **99**, 2272–2283 (2018).

Wang, X. et al. Phylogenetic and functional diversity area relationships in two temperate forests. *Ecography* **36**, 883–893 (2013).

Wiegand, T. & Moloney, K. A. *A handbook of spatial point pattern analysis in ecology*. (Chapman and Hall/CRC press, 2014).

Wiegand, T., May, F., Kazmierczak, M. & Huth, A. What drives the spatial distribution and dynamics of local species richness in tropical forests. *Proc. R. Soc. B* **284,** 20171503 (2017).

Webb, C., & Donoghue, M. Phylomatic: tree assembly for applied phylogenetics. *Molecular Ecology Notes* **5**, 181 – 183 (2005)

Acknowledgments

X.W. was supported by the National Key Research and Development Program of China (2022YFF1300501), the Strategic Priority Research Program of Chinese Academy of Sciences (Grant XDB31030000), the Key Research Program of Frontier Sciences, Chinese Academy of Sciences (Grant ZDBS-LY-DQC019). The Harvard ForestGEO Forest Dynamics plot (Orwig et al. 2022) was funded by the Center for Tropical Forest Science and Smithsonian Institute's Forest Global Earth Observatory (CTFS-ForestGEO), the National Science Foundation's LTER program

(DEB 06-20443, DEB 12-37491, and DEB 18-32210) and Harvard University. Thanks to the many field technicians who helped census the plot and Jason Aylward and Christina McKeown for field supervision, data screening and database management. The FS plot project was supported by the Taiwan Forestry Bureau, the Taiwan Forestry Research Institute, and the Ministry of Science and Technology of Taiwan. Funding for the establishment of the SCBI ForestGEO Large Forest Dynamics Plot was provided by the Smithsonian Global Earth Observatory (SIGEO) initiative, the Smithsonian Institution National Zoological Park, and the HSBC Climate Partnership. We especially thank the numerous technicians, interns, and volunteers of the Conservation Ecology Center at the SCBI who were essential in assisting with plot establishment and data collection. The BCI censuses have been made possible through support of the U.S. National Science Foundation (awards 8206992, 8906869, 9405933, 9909947, 0948585 to S.P. Hubbell), the John D. and Catherine D. McArthur Foundation, and the Smithsonian Tropical Research Institute. We also thank the hundreds of people who contributed to the collection and management of the data from the plots. Funding for the Tyson Research Center (TRC) Forest Dynamics Plot was provided by the National Science Foundation (DEB Awards 1557094 and 2240431 to J.A.M.), the International Center for Advanced Renewable Energy and Sustainability (I-CARES) at Washington University in St. Louis, Tyson Research Center, and the Forest Global Earth Observatory (ForestGEO). We thank the Tyson Research Center staff for providing logistical support, and the more than 100 high school students, undergraduate students, and researchers that have contributed to the project. The 25-ha Long-Term Ecological Research Project at Sinharaja World Heritage Site is a collaborative project of the Uva Wellassa University, University of Peradeniya, the Forest Global Earth Observatory (ForestGEO) of the Smithsonian Tropical Research Institute, with supplementary funding received from the John D. and Catherine T. Macarthur Foundation, the National Institute for Environmental Science, Japan, and the Helmholtz Centre for Environmental Research-UFZ, Germany, for past censuses. The PIs gratefully acknowledge the Forest Department, Uva Wellassa University, and the Post-Graduate Institute of Science at the University of Peradeniya, Sri Lanka for supporting this project, and the local field and lab staff who tirelessly contributed to the repeated censuses of this plot. This work was stimulated by discussions of the working group sNiche (Expanding neo-Chessonian coexistence theory towards a stochastic theory for species rich communities) supported by sDiv, the Synthesis Centre of iDiv (DFG FZT 118). We thank the Kraft lab for valuable feedback on earlier drafts.

Author contributions

T.W., X.W., S. F. and A. H. conceived and designed the project, T.W. implemented the models, conducted the simulations, analysed the results, and prepared figures and tables. T.W., A.H., S. F., X.W. and N.K. led the writing of the manuscript. X.W. assembled and analysed the plot data and conducted the spatial analyses. All other co-authors contributed data, reviewed, approved, and had the opportunity to comment on the manuscript.

Competing interests

The authors declare no competing financial interests.

Additional information

Supplementary Information is available for this paper.

Correspondence and requests for materials should be addressed to T.W. or X.W.

Corresponding authors

Correspondence to thorsten.wiegand@ufz.de or wangxg@iae.ac.cn.

Extended Data Figures

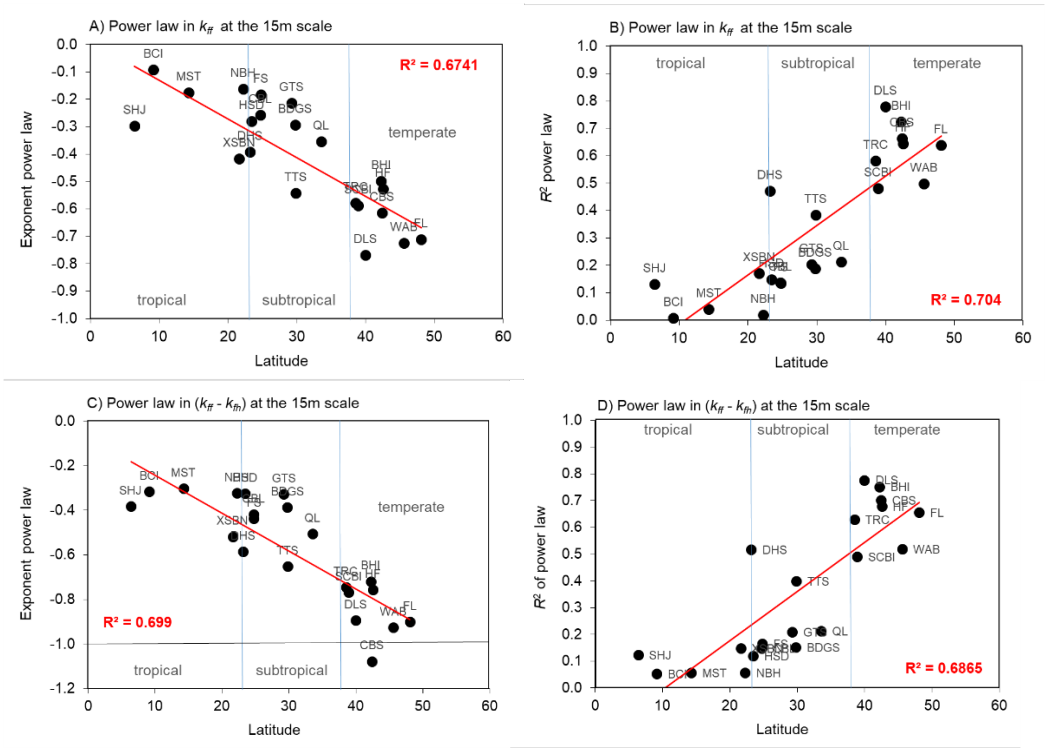

Extended Data Figure 1. Latitudinal gradients in the abundance-aggregation and the corrected abundance-aggregation power laws for a neighbourhood distance of r = 15m. (A) the power law exponent of the scaling of aggregation k_{ff} with abundance N_f, (B) the R^2 for the power laws shown in A), (C) same as A) but for the scaling of (k_{ff} - k_{fh}) with abundance N_f. (D) same as B) but for the scaling of (k_{ff} – k_{fh}) with abundance N_f. Our scale-dependent measures of aggregation k_{ff} and segregation k_{fh} are based on neighbourhood crowding indices that count the number of neighbours within distance r of the focal individual, but each neighbour is weighted by the inverse of its distance to the focal individual. For plot acronyms see Table 1.

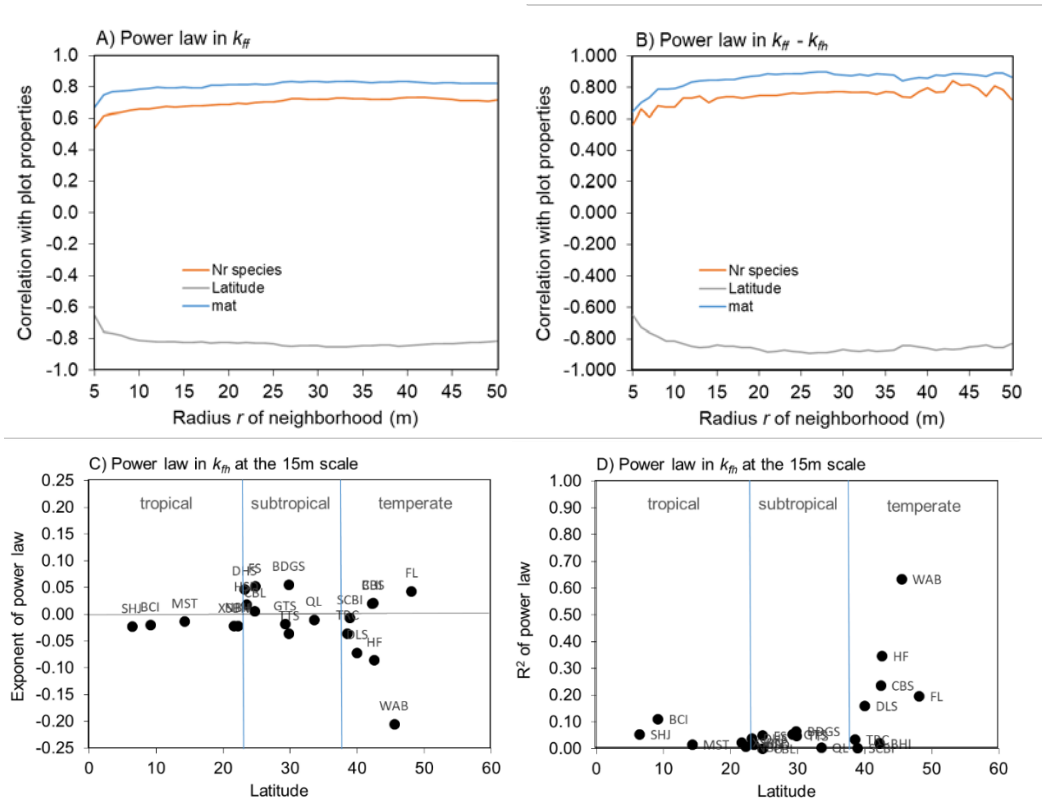

Extended Data Figure 2. **Abundance-dependency of k_{ff} and k_{fh}.** (A) The correlation coefficient between the exponent of the power law and the plot properties species richness, latitude and mean annual temperature (mat) for the power law in aggregation k_{ff} with respect to abundance N_f, (B) the power law in ($k_{ff} - f_{fh}$) with respect to abundance N_f, where k_{ff} is conspecific aggregation and k_{fh} heterospecific segregation. (C) Exponent of the power law of segregation k_{fh} with respect to species abundance N_f for the 21 the ForestGEO data sets. (D) the R^2 of the linear regression between $\ln(k_{fh})$ and $\ln(N_f)$.

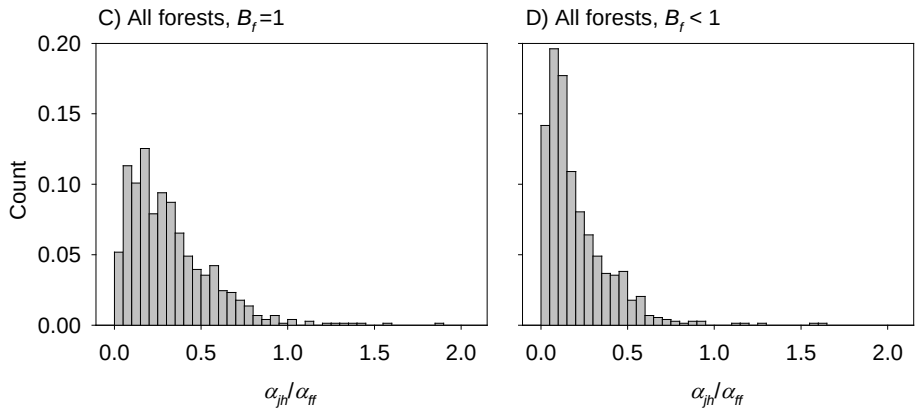

Extended Data Figure 3. Heterospecific population-level interaction coefficients α_{fh} relative to the conspecific population-level interaction coefficients α_{ff} (A) For scenario 1 where con-and heterospecifics compete equally at the individual level (i.e., B_f = 1). (B) For scenario 2 where phylogenetic similarity was used as proxy for the pairwise individual-level interactions coefficients α_{fi}. Only 14 species show values of α_{fh} / α_{fh} > 1.

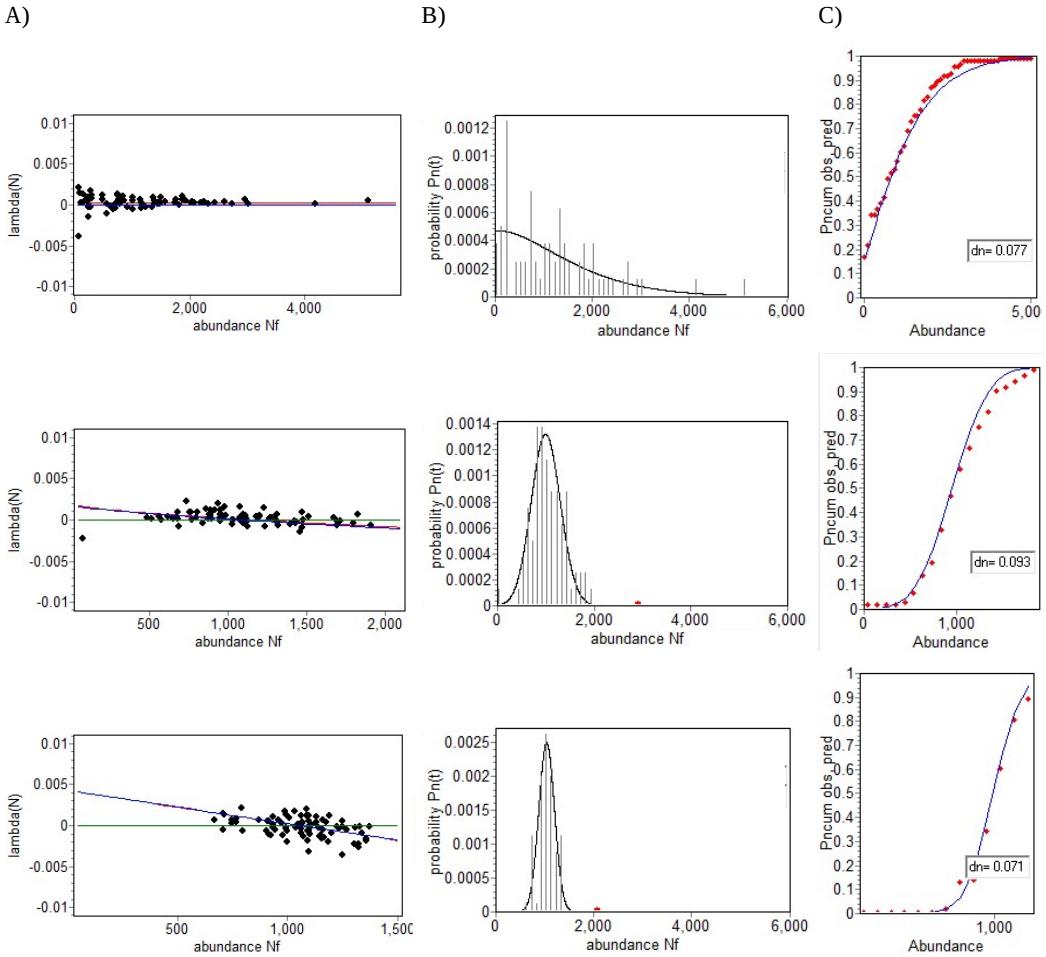

Extended Data Figure 4. The birth-death model predicts the species abundance distribution of individual-based simulations. (A) The average individual fitness (red-blue line) determined from the fitted power-law relationship between ($k_{ff} - k_{fh}$) and N_f (Extended Data Figure 4), the mean value of k_{fh}, the observed total community size J, and the model parameters β_{ff} = 0.02, r_f = 0.1, and s_f = 1.0 (see methods). The black dots show the values of average individual fitness for the different species, given their observed abundance N_f^*, aggregation k_{ff} and segregation k_{fh}. (B) The observed species abundance distribution of the individual-based model after 25,000 years (bars) and the corresponding prediction of the birth-death model (black line), the (scaled) probability $P_n(t)$ that the species has at time t n individuals. (C). The cumulative probability distributions (red dots: observed, blue line: predicted by birth-death model). The individual-based simulation model is a spatially explicit and stochastic implementation of the spatial multi-species model (equation 1), and simulates the dynamics of a community of initially 80 tree species in a given 200 ha plot of a homogeneous environment in 5-year time steps.

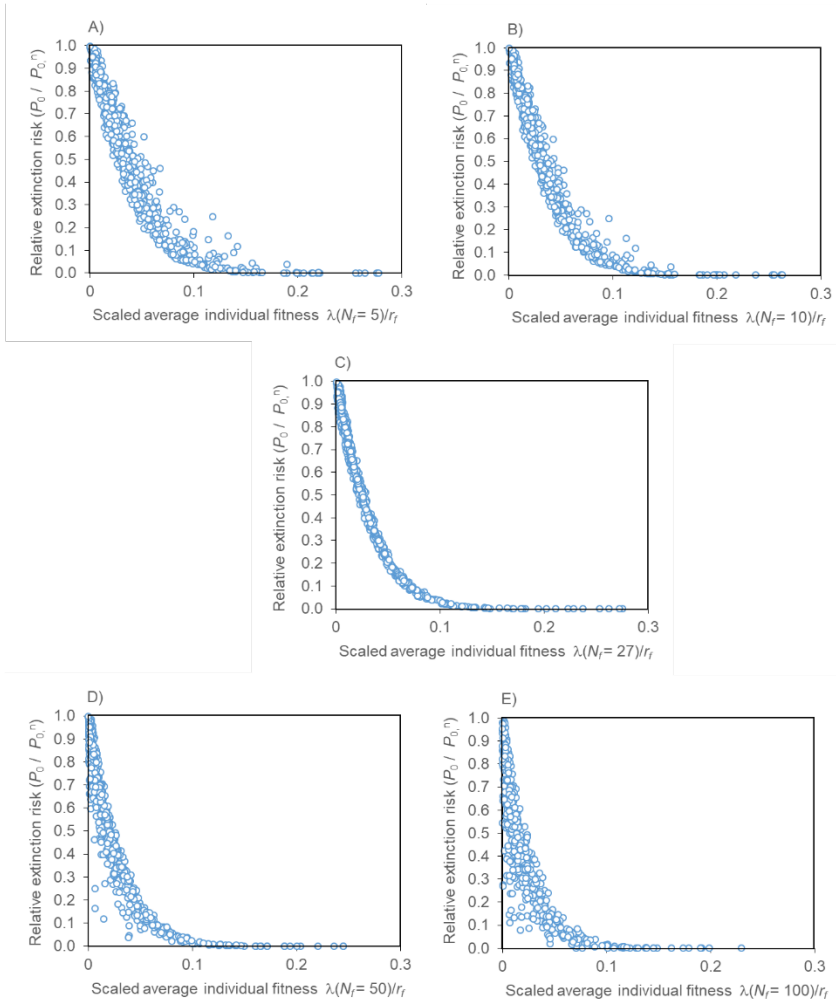

Extended Data Figure 5. Scale collapse of the extinction probability at timestep t = 200 (1000 yrs). We scale the extinction probability $P_0(t, N_0)$ with the expected extinction probability of the neutral model (equation 2a) and the average individual fitness $\tilde{\lambda}_f$ with its maximal possible value r_f. We then plot the relative extinction probability P_0/P_0^n over $\tilde{\lambda}_f(N_f)/r_f$, for different abundance values N_f (A: N_f = 5, B: N_f = 10, C: N_f = 27, D: N_f = 50, E: N_f = 100) to identify the suitable abundance N_s which leads to the scale collapse. For a given value of t we find that only one suitable value of N_f (here N_s = 27), shown in C), leads to a scale collapse and yields an almost deterministic relationship. The data are from scenarios 1 (no niche differences, N_0 = 50).

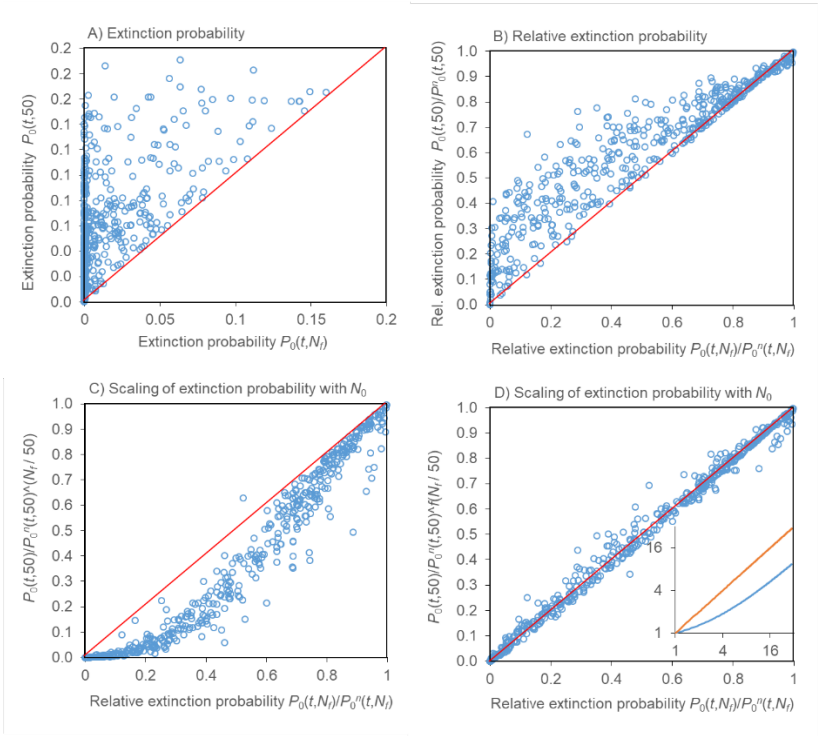

Extended Data Figure 6. Scaling of the relative extinction probability with initial condition N_0 to derive expectations for how spatial mechanisms impact species coexistence in species-rich communities. (A) The extinction probability $P_0(t, 50)$, for time step $t = 200$, plotted over $P_0(t, N_f)$, where $N_f > 50$ is the observed abundance of our 720 study species. The extinction probability, when starting with 50 individuals, is always larger than the extinction probability when starting with the observed N_f individual. (B) Same as A), but for the relative extinction risk $P_0(t, N_0)/P_0^n(t, N_0)$. (C) Scaling of the relative extinction probability for $N_0 = 50$ with exponent $N_f/50$, as suggested by neutral scaling (equation 2). The neutral scaling overestimates the relative extinction probability for $N_0 = N_f$. This is because neutral scaling assumes independence of the fate of each individual, but neighbourhood crowding introduces correlations between the fates of nearby individuals and as consequence, the effective number of individuals (the random equivalent) is lower. (D) Scaling of the relative extinction probability (equation 2b) for $N_0 = 50$ with an exponent that is a function $f(x)$ of $x = N_f/50$, which accounts for the decline in the effective number of individuals. The small inset shows the function $f(x)$ (blue line) and the 1-to-1 line (orange line). This scaling allows us to predict the relative extinction probability, when starting with N_0 individuals, from the relative extinction probability when starting with $N_0 = 50$ individuals. The function $f(x) \approx (0.29\,x + 0.71)$ resulted from fitting our data. We used the extinction probabilities resulting from the birth-death model parameterized for our 720 species for scenario 1 where con- and heterospecifics compete equally. The red lines are the 1-to-1 line.

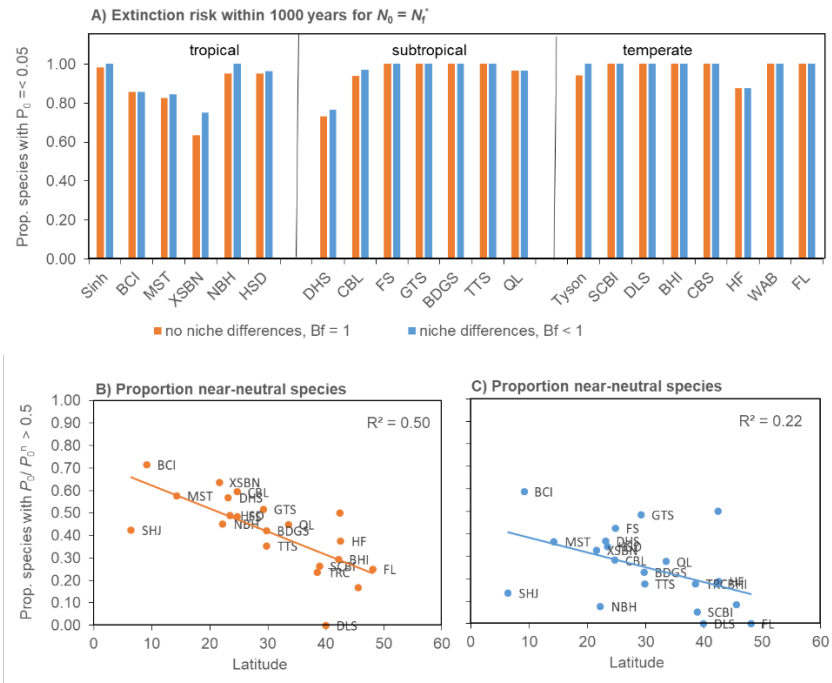

Extended Data Figure 7. Extinction risk within 1000 years, when using the current species abundance as initial population size. (A) Proportion of species with an extinction risk $P_0(t) < 5\%$ within $t = 200$ timesteps (1000 years). Orange: scenario 1 where con- and heterospecifics compete equal at the local scale (i.e., $B_f = 1$), and blue: scenario 2 where we approximate niche differences by phylogenetic dissimilarity (i.e., $B_f < 1$). (B) Geographic variation in the proportion of species that behave near-neutral for scenario (i.e., $P_{N_0,0}(t)/P^{neu}_{N_0,0}(t) > 0.5$) for scenario 1. (C) Same as B), but for scenario 2. The underlying birth-death model (equations 11, 12) assumed that survival was driven by neighborhood crowding.

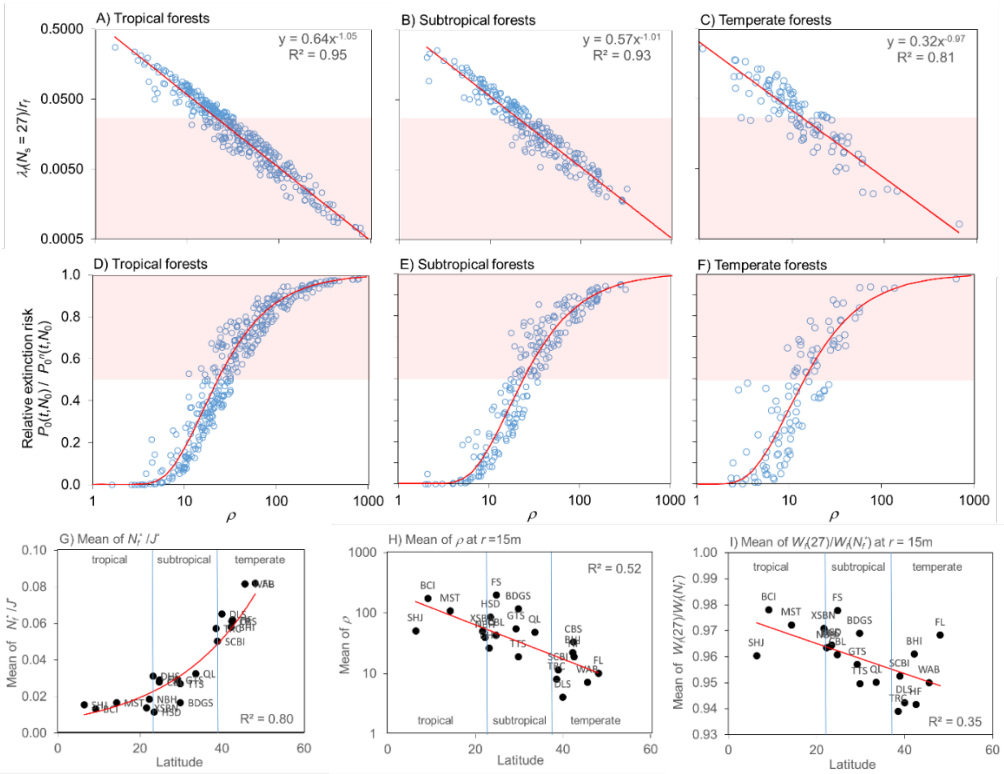

Extended Data Figure 8. Which properties of a species lead to a low extinction risk? (A – C) The scaled average individual fitness $\tilde{\lambda}_f(N_s = 27)/r_f$, parameterized for the different species of tropical, subtropical and temperate forests, plotted over $\rho_f = (J/N_f^*)\, B_f\, k_{fh}/(k_{ff} - k_{fh})$ (equation 15b). The red shaded area indicates near-neutral species with $\tilde{\lambda}_f(N_s = 27)/r_f < 0.025$, a threshold taken from figure 2B. It indicates that the extinction probability of a species is smaller if $\tilde{\lambda}_f(N_s = 27)/r_f$ is relatively larger. (D – F) The same as A – C, but now the relative extinction risk is shown directly in dependency on ρ_f. (G) The mean relative abundance N_f^*/J, which drives the quantity ρ_f, averaged over all species of a given plot shown in dependence on latitude. (H) The mean of the quantity ρ_f in dependence on latitude. (I) The mean of the ratio $W_f(N_f = 27)\ /\ W_f(N_f^*)$ that drives the average individual fitness (eq. 9a). The strong dependency of the scaled average individual fitness on ρ_f suggests that the other factors involved in ratio $W_f(N_f = 27)\ /\ W_f(N_f^*)$, given in equation 14, including the aggregation-abundance relationship, are less important.

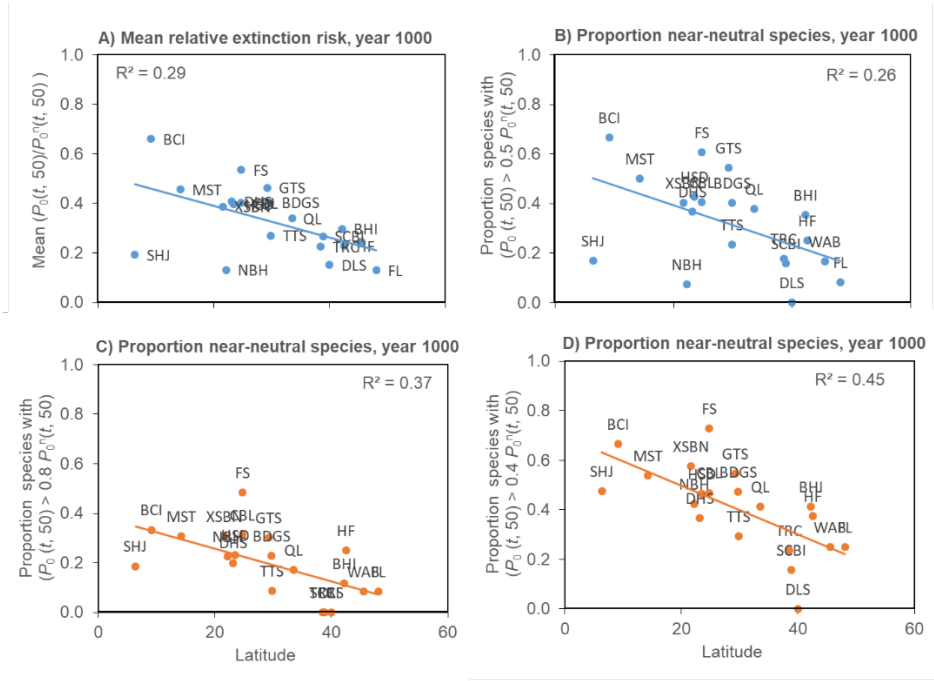

Extended Data Figure 9. Geographic variation in the proportion of near-neutral species. (A) Same as figure 3A, but for scenario 2 assuming niche differences, (B) Same as figure 3B, but for scenario 2 assuming niche differences, (C) Same as figure 3A, but for a threshold of 0.8 to define near-neutral species, i.e., with $P_0(t, N_0) < 0.8\, P_0^n(t, N_0)$. C) Same as figure 3A, but for a threshold of 0.4 to define near-neutral species, i.e., with $P_0(t, N_0) < 0.8\, P_0^n(t, N_0)$.

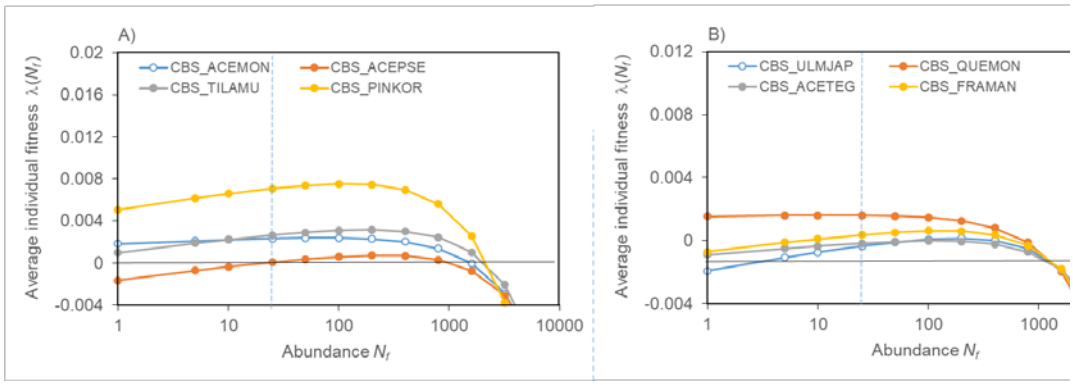

Extended Data Figure 10. Examples of the average individual fitness for the CBS plot for scenario 2 with niche differences (i.e., $B_f < 1$). We assumed that individuals compete at the individual scale more strongly if they phylogenetically more similarity. The CBS plot shows a power law exponent of $b_f = -1.077$, which leads to unstable dynamics if con- and heterospecifics compete equally at the individual scale. However, niche differences allow a few species (ACEMON, TILAMU, PINKOR, ULMJAP, QUEMON) to fulfil the deterministic invasion criterion (equation 9). They are all abundant species that show weak aggregation. The vertical dashed line indicates the value of the average individual fitness (at $N_f = 27$) that determines the extinction risk of a population with initially 50 individuals after 1000 years.

Supplementary Table 1: Characteristics of the selected forest plots.

Plot	Acronym	Latitude	Longitude	Elevation	Forest type	No. species	Individuals ≥10cm dbh	No. species ≥10cm dbh	No. focal species†	Area (ha)	MAT	MAP	Survival rate‡
Sinharaja	SHJ	6.40	80.40	500	tropical	239	17070	167	59	25	22.5	5016	0.913
BCI	BCI	9.15	-79.85	140	tropical	304	20647	238	63 (-10)	50	23.5	2551	0.887
MoSIngTo	MST	14.26	101.22	770	tropical	262	15665		52 (-2)	30	27.1	2100	0.864
Xishuangbanna*	XSBN	21.61	101.57	789	tropical	468	12263	339	52	20	21.8	1493	0.860
Nabanhe	NBH	22.23	100.6	932	tropical	290	8512	221	40 (-2)	20	19.4	1350	
Heishiding	HSD	23.45	111.89	567	tropical-subtropical	245	30992	148	82	50	22.0	1743.8	0.900
Dinghushan*	DHS	23.16	112.51	350	subtropical	210	11906	131	30	20	20.9	1985	0.820
Chebaling	CBL	24.72	114.25	495	subtropical	228	10159	148	32	20	18.8	1468	
Fushan*	FS	24.76	121.56	600–733	subtropical	110	19261	77	33 (-1)	25	18.2	4067	0.929
Gutianshan*	GTS	29.25	118.12	581	subtropical	159	18215	109	33	24	15.3	1963	0.910
Badagongshan	BDGS	29.77	110.09	1406	subtropical	232	25121	186	57	25	15.9	2105	0.940
Tiantong	TTS	29.81	121.78	454	subtropical	154	14967	107	34	20	16.2	1375	0.920
Qinling*	QL	33.54	108.37	1431	temperate-subtropical	121	11698	84	29	25	8.8	908	
Tyson Research Center	TRC	38.52	-90.56	203	temperate	46	6520	38	17	20	12.7	992	
SCBI	SCBI	38.89	-78.15	330	temperate	65	8165	49	19	25	11.6	944	0.920
Donlingshan	DLS	39.96	115.43	1400	temperate	51	9558	39	15	20	4.7	600	0.960
Baihua*	BHI	42.22	128	793	temperate	63	17197	34	17	24	1.8	760	0.930
Changbaishan*	CBS	42.38	128.08	801	temperate	52	9995	34	16	25	2.9	700	0.950
Harvard Forest	HF	42.54	72.18	354	temperate	55	23901	34	16	35	7.8	1050	0.86
Wabikon*	WAB	45.55	-88.80	501	temperate	36	14021	22	12 (-2)	25.2	4.2	805	0.960
Fenglin	FL	48.08	129.12	447	temperate	46	8601	23	12	30	0.5	684	0.890

† The numbers give the number of focal species with at least 50 individuals with dbh >= 10cm, and the number of excluding species (shown in parenthesis) with $k_{ff} < k_{fh}$ and two species at the Wabikon forest located in a patch of successional forest that was logged approximately 40 yr ago.
* Bar code phylogeny, genus level phylogenies were used for all othert plots.
‡ We used a survival rate of 0.9 for the 4 plots without survival data.

Supplementary Table 2: Explanation of important mathematical symbols

Symbol	Meaning
(A) Population level quantities	
$N_{f,t}$, N^*_f	abundance of species *f* at time *t* and corresponding equilibrium abundance.
$J = \sum_i^S N_i^*$	total community size in equilibrium (eq. 6c).
Δt	time step, in our case 5 years, the census interval of the ForestGEO plots.
r_f	average number of offspring of an individual of species *f* within the 5 year census interval. Turnover if species is close to equilibrium (eq. 1).
s_f	background per capita survival rate of species *f* in absence of neighbourhood competition within the 5 year census interval (eq. 1).
$\bar{s}_f$	the average population-level survival rate (eq. 5)
β_{ff}	conspecific individual-level interaction coefficient of the focal species *f*. Defines the strength of negative density dependence (eq. 1).
β_{fi}	individual-level interaction coefficient, measures the negative impact an individual of species *i* has on survival of individuals of the focal species *f*.
β_{fi}/β_{ff}	relative individual-level interaction coefficient, ranges between zero and one. We use phylogenetic similarity as surrogate for β_{fi}/β_{ff}. Large similarity (i.e., $\beta_{fi}/\beta_{ff} \approx 1$ leads to strong competition whereas low similarity ($\beta_{fi}/\beta_{ff} << 1$) leads to weak competition.
A	area of the observation window.
f	focal species.
b_f	exponent of the aggregation-abundance power law (eq. 8).
$\tilde{\lambda}_f(N_{f,t})$	average individual fitness of species *f*, a key quantity that can be derived from the macroscale model (eq. 1).
$W_f(N_{f,t})$	the fitness factor of species *f*, in our case the average of the neighbourhood crowding indices $NCI_k = C_{kf} + I_{kf}$ of the individuals *k* of species *f* (eq. 7b).
(B) quantities for neighbourhood crowding indices	
r	neighbourhood radius: all individuals within distance *R* of a focal individual are counted, we use r = 15m.
k	the focal individual.
NCI_k	the neighbourhood crowding index of individual *k*, it counts the number of individuals within the neighbourhood radius *r* of individual *k*, but weights each neighbour by the inverse of its distance to individual *k*. We decompose NCI_k into separate indices for con- and heterospecific neighbours: $NCI_k = C_{kf} + I_{kf}$

C_{kf}	conspecific crowding index: distance-weighted number of conspecific neighbours within distance r of individual k of the focal species f.
H_{kf}	heterospecific crowding index: distance-weighted number of heterospecific neighbours within distance r of individual k of the focal species f.
I_{kf}	heterospecific interaction crowding index: number of conspecific neighbours within distance r of individual k of the focal species f, weighted by distance and relative individual-level interaction coefficient β_{fi}/β_{ff}.
$\overline{C_{kf}}$, short: C_{ff}	the average conspecific crowding index of species f, can be decomposed into measures of spatial patterns and abundances (eq. 6a).
$\overline{H_{kf}}$, short: H_{fh}	the average heterospecific crowding index of species f, can be decomposed into measures of spatial patterns and abundances (eq. 6b).
$\overline{I_{kf}}$, short: I_{fh}	the average heterospecific interaction crowding index of species f, can be decomposed into measures of spatial patterns and abundances (eq. 6c).
$c = 2\pi\, r/A$	scales population sizes from the plot scale with area A to the neighbourhood scale with area $\pi\, r^2$. The circumference of the neighbourhood is used because each neighbour is weighted by the inverse of its distance to the focal individual.

(C) point pattern quantities

k_{ff}	an index of conspecific aggregation of the focal species f. It is the mean conspecific crowding index C_{ff} (eq. 6a), divided by its expectation for randomly distributed conspecifics. Thus, $k_{ff} > 1$: clustering, $k_{ff} \approx 1$: random pattern, and for $k_{ff} < 1$: regularity.
k_{fh}	an index of segregation or attraction of heterospecifics to the focal species f. It is the mean heterospecific crowding index H_{fh} (eq. 6b), divided by its expectation for independently distributed heterospecifics. Thus, $k_{fh} > 1$: attraction (more than expected heterospecific neighbours), $k_{fh} \approx 1$: independence, and $k_{fh} < 1$: segregation (fewer than expected heterospecific neighbours).
B_f	describes the effect of niche differences, it is I_{fh}/H_{fh}, the average (relative) heterospecific neighbourhood competition strength suffered by the typical individual of species f from one heterospecific individual within its neighbourhood with radius r (eqn. 6c). It indicates how much the competition strength of one heterospecific neighbour differs on average from that of one conspecific neighbour. For $B_f = 1$ con- and heterospecifics compete equally at the local neighbourhood scale.
$PL(N_f)$	the corrected power law relationship between aggregation and abundance (eq. 8).
b_f	exponent of the aggregation-abundance power law (eq. 8).
κ_f	a quantity appearing in the invasion criteria (eq. 11a, 14, 15a).

ρ_f	a quantity appearing in the extended invasion criteria (eq. 15b), dominates the ratio $W_f(N_f)/W_f(N^*_f)$ of the fitness functions that drives the model (eq. 9).

(D) variables of the birth-death model

$P_n(\tau)$	the probability of population size n at small timestep τ.
n	population size.
$\delta\tau$	small time step to iterate the birth-death model, must be selected in a way that occurrence of more than 1 event is very unlikely. We selected $\delta\tau$= 1/4000, thus one 5 year time step Δt of the macroscale model (eq. 9) corresponds to 4000 timesteps $\delta\tau$ of the birth-death model (eq. 12).
b_n	the probability that during the small time step $\delta\tau$ one birth event occurs in a population of n individuals (eq. 12a).
d_n	the probability that during the small time step $\delta\tau$ one death event occurs in a population of n individuals (eq. 12b).
N_0	initial abundance in the birth-death model.
$P_0(t, N_0)$	the probability that a species with initially N_0 individuals will be extinct at time step t.
$P_0^n(t, N_0)$	the extinction probability of the corresponding neutral model with reproduction rate r_f (eq. 2a, Fig. 2a).
$P_0(t, N_0/P_0^n(t, N_0)$	the relative extinction probability, the effects of non-neutral mechanisms (here neighbourhood crowding) on the ability of species to persist in terms of the reduction in the extinction probability relative to that of the corresponding neutral model.
N_s	suitable abundance where the scale collapse of the relative extinction probability with respect to the turnover-scaled average individual fitness occurs (Fig. 2B, Extended Data Fig. 5).
$f(N_1/N_2)$	scaling function of the exponent of the power-law scaling of the relative extinction probability with initial abundance N_2 to the relative extinction probability with initial abundance N_1 (Fig. 2c, Extended Data Fig. 6).

Supplementary Text:

Population-level interaction coefficients

Equation 6 allows us also to determine the community-level interaction coefficients α_{ff} and α_{fh} by rewriting the fitness factor of equation 7 as $W_f = \alpha_{ff}(N_f + \sum_{i \neq f} \frac{\alpha_{fi}}{\alpha_{ff}} N_i) / \beta_{ff}$, which results in the coefficients

$$\alpha_{ff} = c\, \gamma_{ff} \beta_{ff}\, k_{ff} \tag{S1a}$$

$$\alpha_{fh} = c\, \gamma_{f\beta} \beta_{ff}\, (B_f k_{fh}) \tag{S1b}$$

The ratio of the strength of heterospecific competition relative to conspecific competition is then approximately given by

$$\frac{\alpha_{fh}}{\alpha_{ff}} \approx B_f \frac{k_{fh}}{k_{ff}} \tag{S1c}$$

Thus, the community-level conspecific interaction coefficients α_{ff} are not constant, as commonly assumed, but abundance-dependent if aggregation k_{ff} depends on abundance, as observed in our forest dynamics plots (Figure 1). Equation S1c has two extreme cases. First, without spatial structure (i.e., $k_{fh} / k_{ff} = 1$) reduced niche overlap (i.e., $B_f < 1$) makes conspecific competition stronger than heterospecific competition. Second, if con- and heterospecifics compete equally (i.e., $B_f = 1$), conspecific competition is stronger than heterospecific competition if $k_{ff} > k_{fh}$, which is the case for almost all of the species we investigated (Extended Data Fig. 3). If aggregation is independent on abundance (i.e., the α_{ff}'s are constant) and $k_{ff} > k_{fh}$, the effect of conspecific competition, given by $s_f exp(-\alpha_{ff} N_f)$, will vanish for small abundances N_f and stabilize the community dynamics by a rare species advantage if $\alpha_{ff} > \alpha_{fh}$ (Wiegand et al. 2021). However, if aggregation k_{ff} depends negatively on abundance the condition $k_{ff} > k_{fh}$ will be especially fulfilled for species with small abundances, but the population level effect of conspecific competition $s_f exp(-\alpha_{ff} N_f)$ will vanish slower if abundance declines. Thus, the rare species advantage becomes weaker, and in the limit of α_{ff} proportionally to $1/N_f$ (i.e., the exponent $b_f = -1$), there is no rare species advantage at all.

The stochastic invasion criterion

Equation 17 can be used to estimate the extinction risk of a small population with $N_0 = 50$ individuals within 1000 years and is therefore a probabilistic extension of the deterministic invasion criterion of equation 10. For other values of N_0 and t similar expressions exist, as long as N_0 is small enough and t is not too large that the dynamics would approach the quasi-stationary state (where the extinction risk becomes independent on the initial population size).

Equation 14 shows that the deterministic invasion criterion $W_f(N_f)/W_f(N_f^*) < 1$ loses the information on the term ρ_f that is contained in the stochastic invasion criterion of equation 16. However, extended Data Fig. 8A–F show that the quantity ρ_f is a main driver of the ratio $W_f(N_f)/W_f(N_f^*)$ and thereby of the extinction risk. Thus, the quantity ρ_f can be interpreted as an order parameter that measures the degree of stabilization that drives the risk of extinction relative to the corresponding neutral model. The lower the value of $\log(\rho_f)$, the lower the relative extinction risk. For the example of a small abundance of $N_0 = 50$, values of ρ_f roughly smaller than 20 indicate that the stabilization mechanisms included into our model lead to an risk of extinction at least half of that of the corresponding neutral model.

The value of the order parameter ρ_f is driven in our case by three different factors. First, stabilization is increased if the species shows on average a low niche overlap with other species (i.e., $B_f < 1$). Second, stabilization is increased if the species shows higher values of aggregation k_{ff}. Third, the extinction risk depends on the relative abundance of the focal species N_f relative to the total community size J, the larger the abundance of the species, the lower the extinction risk. This is an effect of demographic stochasticity (Lande 1993). Equation 14 and Figure 2D indicate that the remaining variability shown in Extended Data Fig. 8D–F is mainly due to the exponent b_f of the negative relationship between aggregation and abundance, with values of b_f closer to 0 reducing the risk of extinction) and niche overlap.

Spatially-explicit simulation model (adapted from Wiegand et al. 2021)

The individual-based simulations serve two main purposes; first, they are used to verify that the observed patterns (i.e., the abundance-aggregation power law) can emerge in principle from the minimal mechanisms included into the macroscale model, and they are used as "known data" to test if the parameterized birth-death model (equations 12 and 13) is able to predict the simulated abundance distribution correctly.

The model is a spatially explicit and stochastic implementation of the spatial multi-species model (equation 9), and simulates the dynamics of a community of initially S tree species (in our case $S = 80$) in a given plot of a homogeneous environment (in our case 200 ha) in 5-year timesteps adapted to the ForestGEO census interval. Only reproductive (adult) trees are considered, but no size differences.

During a given 5 yr timestep the model simulates first stochastic recruitment of reproductive trees and placement of recruits, and second, stochastic survival of adults depending on the

neighbourhood crowding indices for conspecifics (C_{kf}) and heterospecifics (H_{kf} or I_{kf} depending on the scenario) (but excluding recruits). In the next timestep the recruits count as reproductive adults and are subject to mortality. No immigration from a metacommunity is considered. To avoid edge effects torus geometry is assumed.

The survival probability of an adult k of species f is given by equation (4) and yields $s_{kf} = s_f \, exp(- \beta_{ff} \, (C_{kf} + I_{kf}))$. The two neighbourhood indices C_{kf} and I_{kf} describe the competitive neighbourhood of the focal individual k and sum up all conspecific and heterospecific neighbours within distance r, respectively, but weight them by the inverse of it distance to the focal individual k and by the relative individual-level interaction coefficients β_{fi}/β_{ff}. If con- and heterospecifics compete equally at the individual-scale, we have $\beta_{fi} = \beta_{ff}$.

Each individual produces r_f recruits on average and their locations are determined by a type of Thomas process (Wiegand and Moloney 2014) to obtain a clustered distribution of recruits. In our model, the spatial position of the recruits is determined by two independent mechanisms. First, a proportion $1-p_d$ of recruits is placed stochastically around randomly selected conspecific adults (parents) by using a two-dimensional kernel function (here a Gaussian with variance σ^2). This is the most common way in most spatially-explicit models to generate species clustering. Technically, we first select for each of these recruits randomly one parent among the conspecific adults and then determine the position of the recruit by sampling from the kernel. Second, the remaining proportion p_d of recruits is distributed in the same way around randomly placed cluster centres that are located independently of conspecific adults. We select first for each of these recruits randomly one cluster centre among the cluster centres of the corresponding species, and then determine the position of the recruit by sampling from the kernel.

Characteristics of the model scenarios

The first scenario represents a case of weak aggregation (σ = 67m) where most recruits are placed not too far away from their parents. It results in the power law $PL(N_f) = 6.2 \, N_f^{-0.999}$ with an average individual fitness functions of almost zero for all abundances (Extended Data Fig. 4A, top), and the birth-death mode predicts after 5000 census periods Δt a very wide probability distribution $P_n(t)$ (Extended Data Fig. 4B, top). The second scenario represents realistic aggregation (σ = 15m) with recruits placed in similar proportions around their parents and randomly selected cluster centres. It results in the power law $PL(N_f) = 2.9 \, N_f^{-0.327}$ with a moderate average individual fitness functions at lower abundances (Extended Data Figure 4A, middle), and a much narrower distribution $P_n(t)$ (Extended Data Fig. 4B, middle). The third scenario represents strong aggregation (σ = 10m) with recruits placed only around the

randomly selected cluster centres. It results in the power law $PL(N_f) = 1.6\ N_f^{-0.0013}$ with a high average individual fitness functions at low abundances (Extended Data Figure 4A, bottom) and a narrow distribution $P_n(t)$ (Extended Data Fig. 4B, bottom). In all cases, the probability distribution $P_n(t)$ predicted by the birth-death model matched the abundance distribution of the individual-based simulations after 5000 census periods well (Extended Data Figure 4C).